Temporal and Spatial Satellite Data Augmentation for Deep Learning-Based Rainfall Nowcasting

Özlem Baydaroğlu[1*], Ibrahim Demir[1,2,3]

[1] IIHR – Hydroscience & Engineering, University of Iowa, Iowa City, Iowa, USA
[2] Civil and Environmental Engineering, University of Iowa, Iowa City, Iowa, USA
[3] Electrical and Computer Engineering, University of Iowa, Iowa City, Iowa, USA

[*] Corresponding Author: Özlem Baydaroğlu (ozlem-baydaroglu@uiowa.edu)

Abstract

Climate change has been associated with alterations in precipitation patterns and increased vulnerability to floods and droughts. The need for improvements in forecasting and monitoring approaches has become imperative due to flash floods and severe flooding. Rainfall prediction is a challenging but critical issue owing to the complexity of atmospheric processes, the spatial and temporal variability of rainfall, and the dependency of this variability on several nonlinear factors. Because excessive rainfall is the cause of natural disasters such as floods and landslides, accurate real-time rainfall nowcast is critical for the necessary precautions, control, and planning. In this study, rainfall nowcasting has been studied utilizing NASA Giovanni satellite-derived precipitation products and the convolutional long short-term memory (ConvLSTM) approach, which is a variation of LSTM. Due to data requirements of deep learning-based prediction methods, data augmentation is performed using interpolation techniques. The study utilized three types of satellite-derived rainfall data, including spatial, temporal, and spatio-temporal interpolated rainfall data, to conduct a comparative analysis of the results obtained through nowcasting rainfall. This research examines two catastrophic floods that transpired in Türkiye Marmara Region in 2009 and Central Black Sea Region in 2021, which are selected as the focal case studies. It also explores the suitability of a nowcast model for various flood events, while also examining the impact of data augmentation on the nowcast.

Keywords: Rainfall, flood, nowcasting, deep learning, data augmentation, interpolation.

---

1. Introduction

Precipitation is one of the most difficult components of the hydrological cycle to predict. The forecasting of precipitation is a challenging task due to its spatial and temporal variability, which is influenced by a multitude of factors including pressure, temperature, wind speed, and direction. The accuracy of precipitation forecasting is heavily reliant on the sub-grid scale parameterization of the precipitation formation process. However, the resolution of simulated atmospheric dynamics and sensitivity to initial conditions impose limitations on sub-grid parameterizations, as evidenced by previous studies (Pappenberger et al., 2005; Buizza et al., 1999; Downtown and Bell, 1988; Harrison et al., 1999). According to Tian et al. (2019), rainfall forecasting is exceedingly difficult to accomplish in the majority of arid regions.

In addition to the difficulty and intricacy of precipitation forecasting, it is of critical significance in a variety of fields, particularly water sustainability. Natural disasters such as floods and landslides are caused by excessive precipitation. The implementation of accurate precipitation predictions enables the adoption of protective and preventive measures against potential disasters, as well as the development of necessary planning (Yildirim and Demir, 2022). Insufficient rainfall results in drought, which can lead to scarcities in food supply, outbreaks of illnesses, and economic setbacks over an extended period (Islam et al., 2023; Yeşilköy and Şaylan, 2022; Yesilkoy, 2020). To ensure adequate preparedness and strategic foresight, it is imperative to assess both surplus and deficit precipitation levels (Zhao et al., 2018; Gao et al., 2019). The precise prediction of precipitation holds significant importance for the purposes of agricultural irrigation and planning of water distribution (Weesakul and Lowanichchai, 2005).

The achievement of adequate food production and the maintenance of its sustainability can only be realized through the methods outlined in previous studies (Zambrano et al., 2019; Dhekale et al., 2018; Tian et al., 2019). The importance of predicting precipitation is widely recognized in the development and arrangement of water distribution systems, as well as in the scheduling of mining operations. The significance of its forecasting in urban areas lies in its profound influence on infrastructure (Alabbad and Demir, 2022), traffic, sewerage networks, water infrastructure (Beck et al., 2010) and various other human activities, as highlighted by Hung et al. (2009). Furthermore, the development of flood information systems has gained significant prevalence in recent times (Li and Demir, 2022). The creation of precipitation prediction models and their integration into these systems has become a crucial undertaking (Sit et al., 2021a). Interactive interfaces enable the computation of potential flood scenarios (Sermet and Demir, 2022), taking into account river contributions resulting from precipitation, as demonstrated in previous studies (Demir et al., 2015; Zahmatkesh et al., 2019).

Deep learning is an artificial intelligence methodology that has demonstrated significant accomplishments across different fields. The present technique is a machine learning approach that finds application in diverse domains such as biometric authentication techniques like fingerprint and voice recognition, computer vision and natural language processing (Sermet and Demir, 2021), iris recognition, and cancer cell identification. The distinguishing characteristic of this approach in contrast to conventional techniques is its superior computational capability, which

is attributable to its intricate and multi-layered architecture, as well as its capacity to handle substantial volumes of data. The application of deep learning techniques in the context of environmental issues is a relatively recent development (Bayar et al., 2009; Sit et al., 2021b; Li and Demir, 2023). These methods have been employed in solar energy forecasting by Sun et al. (2019), strawberry production prediction by Chen et al. (2019), ozone estimation by Eslami et al. (2019), estimating water needs by Guo et al. (2018), river water level estimation by Liang et al. (2018), wind energy forecasting by Wang et al. (2017). Additionally, several researchers including Ayzel et al. (2018), Boonyuen (2018), Akbari Asanjan (2018), Li et al. (2018), Weesakul (2018), and Hernandez et al. (2016) have employed deep learning algorithms for precipitation estimation and have achieved successful results.

The Convolutional Neural Network (CNN) is an innovative method that surpasses the constraints of conventional machine learning methodologies in predictive modeling. The formation of feature maps is achieved through the utilization of linear convolution filters in conjunction with nonlinear activation functions within convolution layers. Long Short-Term Memory (LSTM) networks are a type of artificial neural network that were originally introduced by Hochreiter and Schmidhuber (1997) and have since undergone further development through various contributions. There exist memory structures that are conducive to the acquisition and retention of information over extended periods of time. In the context of Artificial Neural Networks (ANNs), the ability to establish connections between past information and the current time step is limited when dealing with long-term dependencies. The LSTM model was specifically developed to address this particular issue, as documented by Hochreiter and Schmidhuber (1997) and Olah (2015). Shi et al. (2015) proposed Convolutional LSTM (ConvLSTM) as a modified version of LSTM that incorporates the convolution operation within the LSTM cell. This modification aims to enhance the accuracy of spatial data modeling.

Augmenting the quantity of data points, specifically by producing synthetic data, is a valuable strategy for enhancing prediction accuracy and achieving superior analytical outcomes. Data augmentation techniques have become increasingly prevalent (Demiray et al., 2021; Sit et al., 2021c) in response to the substantial data requirements of machine learning algorithms. The aforementioned techniques encompass conventional spatial (Lucas et al., 2022), temporal (Wang, 2020), and spatiotemporal (Chen, 2021; Skoulikaris et al., 2022) approaches, in addition to deep learning methodologies (Kumar et al., 2021; Sit et al., 2023; Demiray et al., 2023). The selection of an appropriate interpolation technique has critical significance and should be based on the inherent properties of the data (Burrough and McDonnell, 2015). They stated that most interpolation methods produce equivalent outcomes when data is abundant. In mountainous regions, data collection is limited and measurements for certain variables may exhibit significant variations even at spatial scales that are comparatively small (Collins, 1995). Several interpolation techniques, including bilinear (Plouffe et al., 2015), bicubic (Peng et al., 2019), nearest neighbor (Lakew and Moges, 2021), distance weighted average (Liu et al., 2020), and kriging (Lucas et al., 2022) have been employed to augment precipitation data.

Several studies have been conducted on rainfall prediction using machine learning techniques. In their study, Adaryani et al. (2022) employ a hybrid model, namely PSO-SVR, that integrates particle swarm optimization (PSO) and support vector regression (SVR) techniques, as well as LSTM and CNN approaches, to forecast rainfall depth for both 5-minute and 15-minute ahead. They reveal that the PSO-SVR and LSTM methodologies exhibited comparable or superior performance to that of CNN. Amini et al. (2022) build a deep neural network architecture intended for the purpose of nowcasting rainfall with a lead time of 5 minutes. To enhance the precision of deep neural networks, they are integrated with the projections of Numerical Weather Forecast (NWP) models through the application of three ensemble models, namely bagging, random forest, and adaptive boosting. The findings indicate that the ensemble models exhibited a higher level of accuracy, surpassing that of deep neural networks by a minimum of 10% in the majority of rainfall occurrences.

The ConvLSTM-based flood index (Deo et al., 2015) forecasting model is developed by Moishin et al. (2021) to assess the likelihood of flood occurrences at forecast horizons of 1, 3, 7, and 14 days. The findings demonstrate that the flood model based on ConvLSTM outperforms the benchmark techniques. Kumar et al. (2020) introduces a framework for nowcasting short-term precipitation events using satellite data. The model is trained using ten sets of NASA IMERG precipitation data, each consisting of 30-minute intervals. The neural network model that underwent training made a prediction regarding the eleventh instance of precipitation within a series of ten such instances. Iterative utilization of predicted precipitation data is employed for nowcasting precipitation with a lead time of up to 150 minutes. The model exhibits accuracy scores of 0.93 and 0.87 for lead times of 30 minutes and 150 minutes, respectively. Chen et al. (2022) devise a LSTM model based on deep learning techniques to predict the distribution of monthly rainfall. The authors conducted a comparative analysis of the LSTM model's performance against a data-driven random forest (RF) model. The findings indicate that the LSTM model exhibits higher accuracy compared to the Random Forest (RF) model in predicting the distribution of rainfall.

Chen et al. (2022) introduced a two-stream convolutional LSTM architecture, comprising a short-term sub-network and a long-term sub-network, for the purpose of nowcasting precipitation. This model employs collaborative utilization of networks to effectively capture the rainfall data heterogeneity. Moreover, a novel memory cell is devised to capture long-range dependencies spatially and temporally. The model produces quite good outcomes, according to the experimental findings. Chen et al. (2022) developed a model for short-term flood prediction. The model incorporates CNN for image processing and LSTM for collecting spatiotemporal characteristics of hydrological data. Interpolated and aggregated rainfall and flow data train the model. They said that the ConvLSTM model exceeded other approaches in three statistical measures.

The intricate and complex characteristics of atmospheric phenomena, which are both nonlinear and multivariable in nature (Baydaroğlu and Koçak, 2014), pose significant challenges to the accurate long-term prediction of rainfall. The present investigation involves rainfall nowcast over a period of 12-time steps, which is equivalent to 6 hours. It examines two flooding events in the

Marmara and Central Black Sea regions in Türkiye through four different datasets and compares the nowcasts' results. The first approach relies solely on raw rainfall satellite-derived rainfall data, while the second, third and fourth incorporate spatially, temporally, and spatiotemporally augmented data, respectively.

The paper is structured as follows: Section 2 provides an overview of the materials and methods employed in the investigation, while Section 3 outlines the results and subsequent discussion, and Section 4 provides a summary conclusion and future suggestions.

2. Materials and Methods

2.1. Study Area

This investigation scrutinizes two catastrophic flood incidents that occurred in distinct years within the Marmara and Central Black Sea regions of Türkiye, which is a country between 26 and 45° E meridians and 36 and 42 °N parallels, as seen in Figure 1.

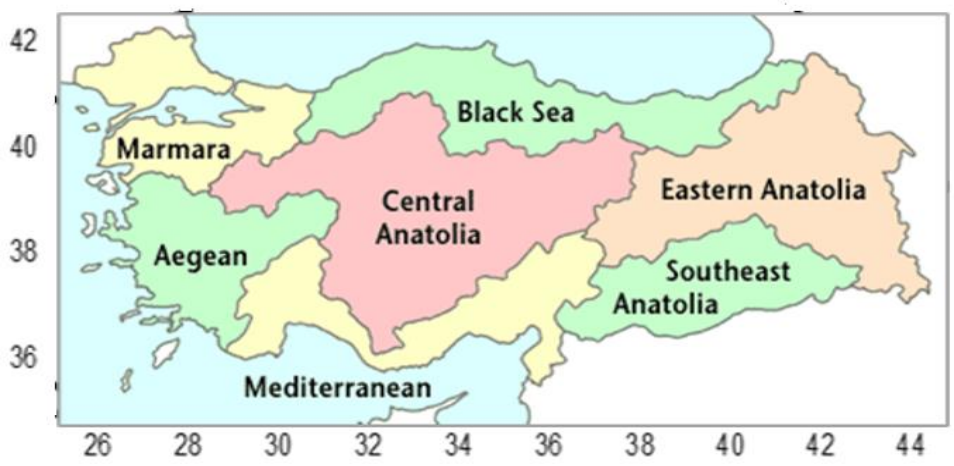

Figure 1. Türkiye regions map.

The flood incident that transpired in the Marmara Region from September 6 to 9, 2009 had a significant impact on a considerable portion of the region, particularly cities Tekirdağ and İstanbul, resulting in fatalities and property damage. The flooding persisted for a duration of approximately four days, with the highest rainfall levels recorded on September 8th, 2009. Figure 2 presents the total amount of rainfall observed on the specified date.

The flood event that occurred in the Central Black Sea area between August 8 and 12, 2021 had a notable effect on a substantial portion of the region, specifically in cities Kastamonu, Sinop, and Bartın, leading to loss of life and damage to property. The flooding endured for a span of roughly five days, with the most elevated amounts of rainfall shown on August 11th, 2021. The data presented in Figure 3 depicts the total rainfall levels observed in the Central Black Sea Region, specifically in Kastamonu, Sinop, and Bartın, on August 11, 2021.

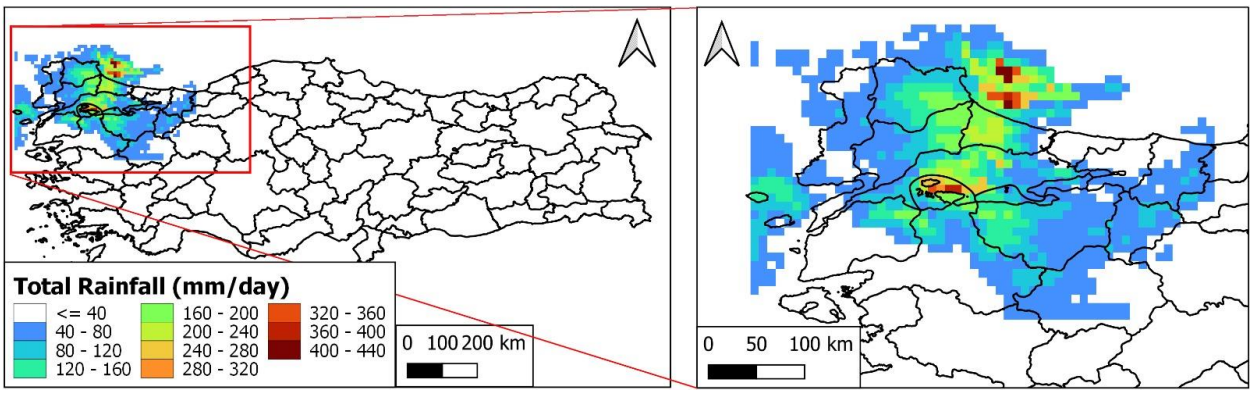

Figure 2. Total rainfall amount in the Marmara Region on September 8, 2009 (Tekirdağ and İstanbul)

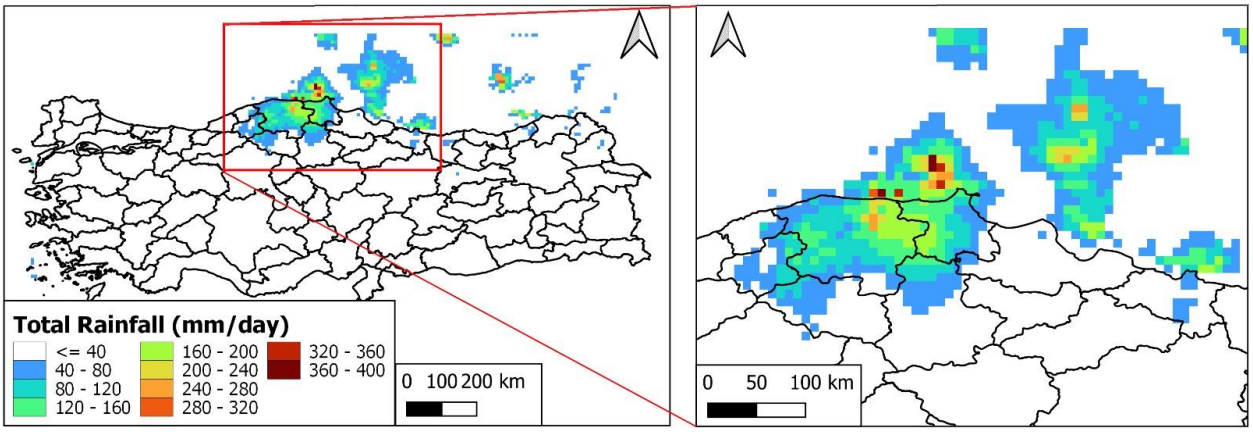

Figure 3. Total rainfall amount in the Central Black Sea Region on August 11, 2021 (Kastamonu, Sinop, and Bartın).

This research examines the floods that occurred in the Marmara and Black Sea Regions, utilizing it as case studies. The analysis involves the scrutiny of satellite imagery pre and post the flood event, with a focus on identifying successive images that depict precipitation. NetCDF-formatted data that corresponds to satellite imagery captured during the precipitation periods are used to construct the ConvLSTM model. The data, acquired from NASA Giovanni (Goddard Interactive Online Visualization and Analysis Infrastructure), includes multi-satellite precipitation estimate with gauge calibration - Final Run (suggested for general use) (GPM_3IMERgHH_v06). The spatial and temporal resolutions of the precipitation data (mm/h) are 0.1° x 0.1° and half hour (30 minutes), respectively.

2.2. Data Augmentation Methodology

The augmentation of data involves the utilization of diverse techniques for spatial and temporal interpolation. The current study utilizes various interpolation methods, including nearest neighbor, bilinear, bicubic, distance weighted average, first and second order conservative and largest area fraction techniques to augment spatial data. Additionally, linear interpolation is employed to

augment temporal data. One of the most straightforward techniques is the nearest neighbor algorithm, which assigns the value of the nearest existing data point to a new point (Parker et al., 1983). The bilinear interpolation algorithm relies on neighboring points closest to the pixel point, which are then weighted to calculate the average pixel value. The determination of weight is contingent upon the spatial separation between the interpolation point and its closest point (Sa, 2014). Bicubic interpolation considers 16 pixels in the closest 4x4 neighborhood of known pixels. These are at different distances from the unknown pixel; so, closer pixels are weighted more heavily.

The utilization of bicubic interpolation algorithms results in the production of images that exhibit greater sharpness in comparison to those generated by nearest neighbor and bilinear interpolation techniques (Parsania and Virparia, 2016). The distance-weighted average method is a statistical technique used to determine the central tendency of a dataset. In this method, the weighting coefficient for each data point is computed as the inverse of the sum of distances between that data point and all other data points. The primary goal of first- and second-order conservative interpolation techniques is to preserve the integral of the data field throughout the interpolation process, spanning from the source to the destination (Shah et al., 2023). The largest area fraction method is predicated upon the identification of the component possessing the greatest proportion of area within each target grid cell. Linear interpolation involves the computation of a new point that is positioned linearly between two pre-existing points.

2.3. Convolutional Long Short-Term Memory (ConvLSTM)

Shi et al. (2015) proposed ConvLSTM as a method for precipitation nowcasting. One notable characteristic that sets ConvLSTM apart from other techniques is that its inputs, cell outputs, hidden states, and gates are all represented as 3D tensors, where the final two dimensions correspond to spatial dimensions. The ConvLSTM model predicts the forthcoming state of a specific cell within a grid by utilizing the previous states and inputs of its adjacent neighbors. The aforementioned outcome is attained through the utilization of a convolution operator during the transitions from state-to-state and input-to-state.

The ConvLSTM model involves inputs $X_1, \ldots, X_t$, cell outputs $Y_1, \ldots, Y_t$, hidden states $H_1, \ldots, H_t$, gates; input gates i_t, forget gates f_t, output gates o_t, and memory cell as c mathematical operators '$*$' convolution and '$\circ$' Hadamard product. The fundamental equations of the ConvLSTM model are expressed as follows:

$$i_t = \sigma(W_{xi} * X_t + W_{hi} * H_{t-1} + W_{ci} \circ Y_{t-1} + b_i) \quad (1)$$

$$o_t = \sigma(W_{xo} * X_t + W_{ho} * H_{t-1} + W_{co} \circ Y_{t-1} + b_o) \quad (2)$$

$$f_t = \sigma\left(W_{xf} * X_t + W_{hf} * H_{t-1} + W_{cf} \circ Y_{t-1} + b_i\right) \quad (3)$$

$$Y_t = f_t \circ Y_{t-1} + i_t \circ tanh(W_{xc} * X_t + W_{hc} * H_{t-1} + b_c) \quad (4)$$

$$H_t = o_t \circ \tanh(Y_t) \quad (5)$$

The selection of hyperparameters is considered to be the most crucial process in the prediction using deep learning. The optimal hyperparameter varies depending on the specific characteristics of each dataset. Failure to choose the suitable hyperparameter may result in inadequate prediction accuracy or an overfitting problem. The likelihood of encountering overfitting is notably elevated, particularly in predictions derived from limited datasets (Zhang, 2018). The problem of overfitting can be defined as an algorithm that exhibits a tendency to learn in a manner that emulates a verbatim replication of the data, thereby deviating from the overarching structure of the data. To address these problems, it is essential to carefully choose appropriate parameters and, in cases where data quality is suboptimal or the quantity of data is insufficient, augment the data points for predictions.

Table 1 presents the hyperparameters utilized in the study. The utilization of the Adam (adaptive moment estimation) optimizer, an algorithm based on gradient descent that integrates the advantageous characteristics of AdaGrad and RMSProp algorithms, has proven to be effective in rainfall nowcasting and the gradual convergence to the minimum of the loss function (Amini et al., 2023). Additionally, it encompasses outliers (Kim and Han, 2020). The Nadam algorithm, which combines Adam and Nesterov's accelerated gradient (NAG) algorithms (Timothy, 2016; Gad et al., 2021), has been demonstrated to exhibit superior predictive performance compared to Adam in some situations (Halgamuge et al., 2020). The optimizers utilized in the study were Nadam and Adam for Marmara and Central Black Sea regions, respectively.

The Rectified Linear Unit (ReLU) activation function has been observed to mitigate the issue of vanishing gradient. Activation functions such as ReLU and its derivatives, including Leaky ReLU, are frequently employed in the field of deep learning (Moishin et al., 2021; Kumar, 2021; Amini et al., 2023). ReLU provides fixed derivatives in positive values that allow the training process to continue even when input values are extreme (Kim & Han, 2020). ReLU and Leaky ReLU were used in the model as activation functions. A notable limitation of the ReLU function is its characteristic of having a gradient of zero for inputs that are non-positive. This property renders a considerable number of neurons unresponsive to adaptation, leading to their inactivity and consequent classification as "dead" neurons. This issue can be alleviated through suitable initialization techniques and by employing small learning rates (Zhang, 2018). Consequently, learning rates of 0.001 and 0.0001 were utilized.

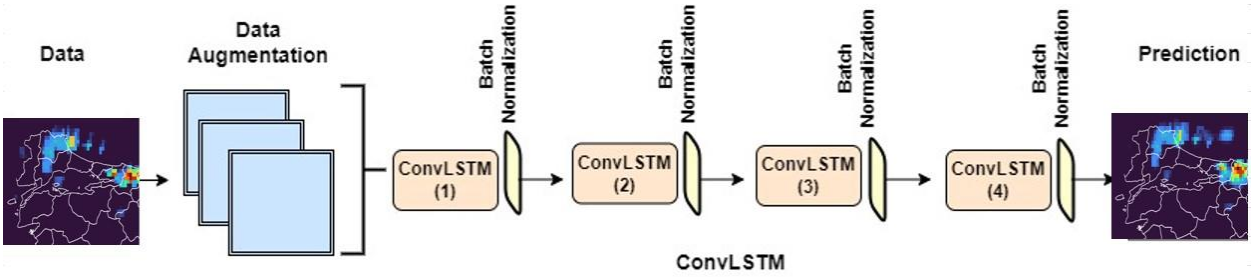

Figure 4. Schematic of the ConvLSTM model.

The implementation of dropout is a crucial aspect in the realm of deep learning. It has the ability to efficiently mitigate overfitting. Conversely, an excessive value of dropouts has the potential to diminish the effectiveness of training (Zhang, 2018). To ascertain the dropout value that yields the minimum loss, a range of dropout values was experimented with, starting from 0.1 and progressing to 0.9. Likewise, various filter numbers (16, 32, 64, and 128) were tested to determine the quantity of filters that result in the least amount of loss. Various batch sizes ranging from 2 to 64 were subjected to testing due to the limited size of the dataset. The experiment involved testing epoch values of 10, 50, and 100. The schematic of the ConvLSTM model is depicted in Figure 4.

All batch sizes listed in Table 1 were tested, and the study was subsequently conducted based on the batch sizes that yielded the most optimal outcomes. For instance, in cases where a batch size of 16 is deemed appropriate for processing data, the model may encounter difficulties in its maintenance when the same data is subjected to spatial augmentation, primarily due to insufficient RAM resources. In such cases, reduced epoch numbers, batch sizes and small learning rates were used to mitigate overfitting issues arising from limited datasets. In addition, a simplistic model was developed to minimize overfitting issues owing to the small datasets.

Table 1. The hyperparameters used in the study.

Hyperparameters & performance criteria	**Options & Ranges**
Optimizer	Adam, Nadam, AdaGrad, RMSProp, Adamax, SGD, Adadelta
Activation function	ReLU, Leaky ReLU, Sigmoid, Tanh
Learning rate	0.001, 0.0001
Dropout	0.1,0.3,0.5,0.7, 0.9
Filter numbers	16,32,64,128
Batch size	2, 4,8,16, 32, 64
Batch normalization	✓
Epochs	10,50,100
Performance criteria	RMSE

The 2D map was subjected to convolutions using a filter size of 5x5. Three filters were employed, and the resulting output was subsequently processed through the Rectified Linear Unit (ReLU) activation function. Following the rectified linear unit (ReLU) activation function, the resulting output undergone additional batch normalization, followed by the application of a dropout rate of 0.1. Subsequently, the following layers executed an identical convolutional operation utilizing filters of dimensions 3x3. The mean squared error (MSE) that is commonly employed as a loss function in conjunction with the Adam or Nadam optimizer was utilized. The learning rate was maintained at a value of 0.0001. In addition, all nowcasting tasks were done for a time frame ranging from 1 to 6 hours.

In this study, the Python programming language was used with the Keras and TensorFlow libraries. The study utilized Google Colab Pro+ as its computational platform. The ConvLSTM model was trained and validated with Python 3 Google Engine backend (TPU) and 35.24 GB RAM. The study's findings were unable to be obtained in certain instances of utilizing augmented data in spatial and temporal contexts due to insufficient RAM capacity.

3. Results and Discussion

One of the primary challenges encountered in the field of rainfall nowcast studies utilizing deep learning techniques is the limited availability of data. This study seeks to investigate the impact of augmenting data using various interpolation methods on the ConvLSTM rainfall nowcast model that has been developed. The present study examines two distinct flood events in the Marmara and Black Sea Regions utilizing satellite data. These regions experienced floods at different times. Furthermore, these geographical areas exhibit distinct orographic formations and are subject to varying air mass influences.

3.1. Marmara Region Flooding

The Marmara Region exhibits the largest population density among, thus leading to significant urbanization. The prolonged and continuous precipitation over a span of four days resulted in highly destructive consequences. During the initial stage of the study, satellite data was employed to evaluate the efficacy of the rainfall nowcast model that was developed. Subsequently, the data resolution was enhanced with the implementation of eight interpolation techniques, encompassing spatial, temporal, and spatiotemporal dimensions. The findings were compared by generating rainfall nowcasts using augmented datasets.

3.1.1. Data Augmentation

Nearest neighbor, linear, bilinear, bicubic, distance weighted average, largest area fraction and, first and second order conservative interpolation techniques were used as data augmentation approaches. The Climate Data Operator (CDO) tool was utilized in all interpolation calculations.

3.1.1.1. Spatial Data Augmentation

The process of augmenting spatial data was conducted by employing various interpolation techniques, including nearest neighbor, bilinear, bicubic, distance-weighted average, largest area fraction, as well as first- and second-order conservative interpolation methods. Figure 5 presents the rainfall data observed during the time interval from 11:30 to 12:00 a.m. on September 8, 2009. The spatial resolution of the rainfall data provided is 0.1° x 0.1°. In the spatial augmentation component of the investigation, the spatial resolution of the rainfall data was increased via interpolation methods, resulting in a spatial resolution of 0.5°x0.5°, 0.025°x0.025° and 0.0125°x0.0125° (see Fig. 6-12). The suitability of bilinear and first-order conservative techniques for interpolating this data is evident from Figures 6–12.

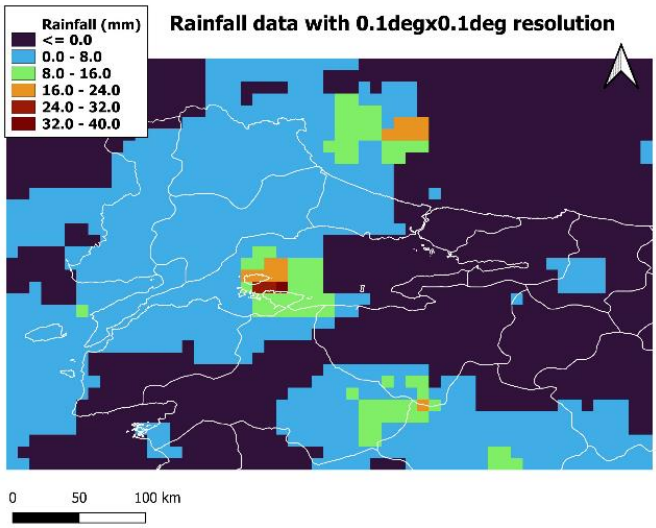

Figure 5. For September 8, 2009, between 11:30-12:00 a.m., rainfall data with 0.1° x 0.1° spatial resolution.

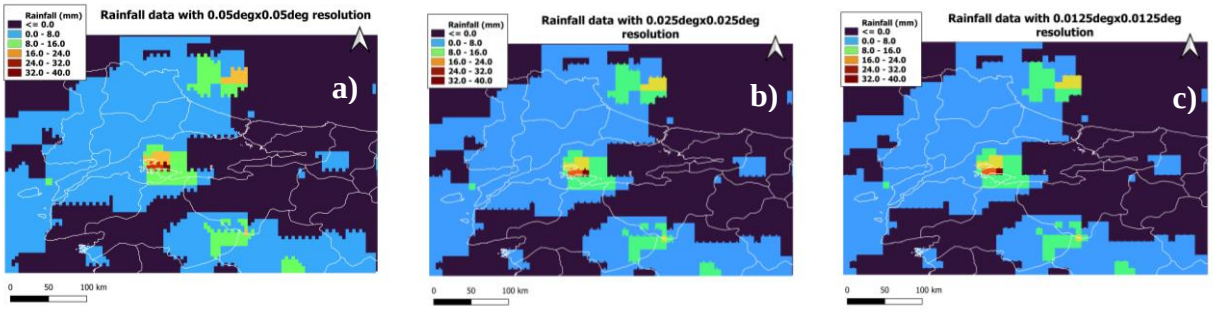

Figure 6. For September 8, 2009, between 11:30-12:00 a.m., (a) Spatially augmented satellite data with 0.05° resolution (x4 higher resolution) (b) Spatially augmented satellite data with 0.025° resolution (x16 higher resolution) (c) Spatially augmented satellite data with 0.0125° resolution (x64 higher resolution) using nearest neighbor interpolation.

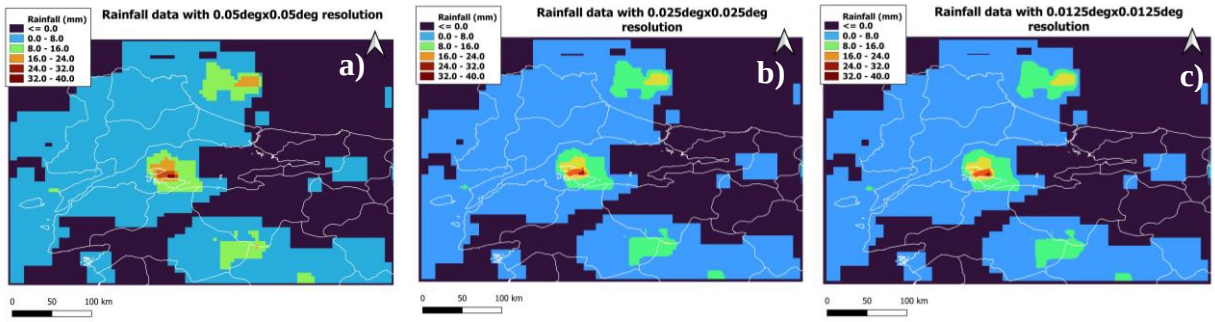

Figure 7. For September 8, 2009, between 11:30-12:00 a.m., (a) Spatially augmented satellite data with 0.05° resolution (x4 higher resolution) (b) Spatially augmented satellite data with 0.025° resolution (x16 higher resolution) (c) Spatially augmented satellite data with 0.0125° resolution (x64 higher resolution) using bilinear interpolation.

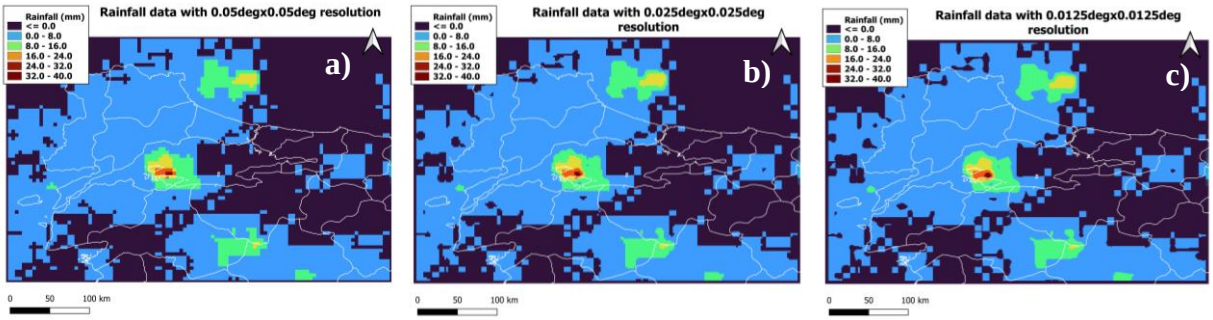

Figure 8. For September 8, 2009, between 11:30-12:00 a.m., (a) Spatially augmented satellite data with 0.05° resolution (x4 higher resolution) (b) Spatially augmented satellite data with 0.025° resolution (x16 higher resolution) (c) Spatially augmented satellite data with 0.0125° resolution (x64 higher resolution) using bicubic interpolation.

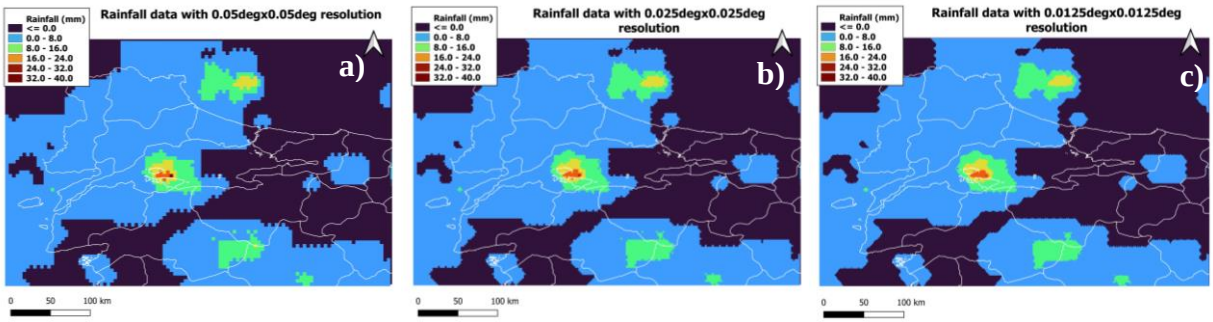

Figure 9. For September 8, 2009, between 11:30-12:00 a.m., (a) Spatially augmented satellite data with 0.05° resolution (x4 higher resolution) (b) Spatially augmented satellite data with 0.025° resolution (x16 higher resolution) (c) Spatially augmented satellite data with 0.0125° resolution (x64 higher resolution) using distance weighted average interpolation.

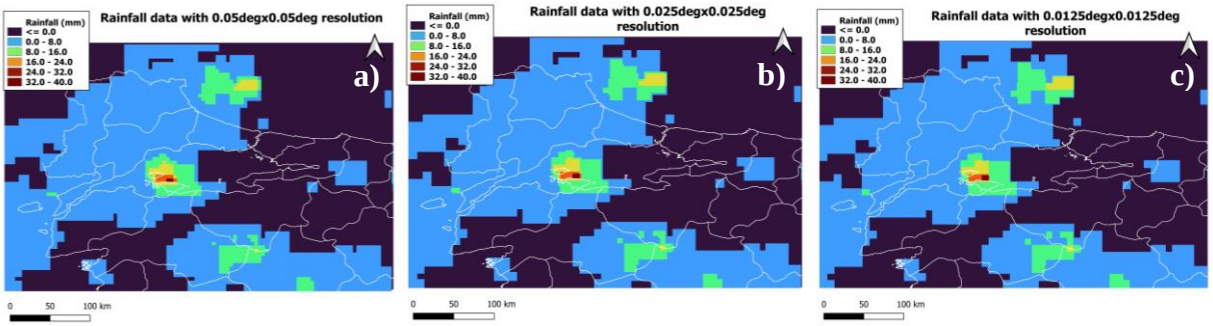

Figure 10. For September 8, 2009, between 11:30-12:00 a.m., (a) Spatially augmented satellite data with 0.05° resolution (x4 higher resolution) (b) Spatially augmented satellite data with 0.025° resolution (x16 higher resolution) (c) Spatially augmented satellite data with 0.0125° resolution (x64 higher resolution) using first order conservative interpolation.

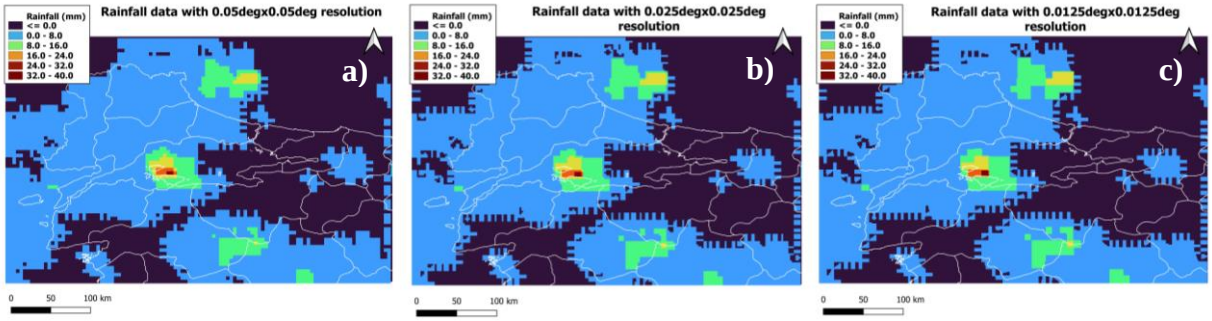

Figure 11. For September 8, 2009, between 11:30-12:00 a.m., (a) Spatially augmented satellite data with 0.05° resolution (x4 higher resolution) (b) Spatially augmented satellite data with 0.025° resolution (x16 higher resolution) (c) Spatially augmented satellite data with 0.0125° resolution (x64 higher resolution) using second order conservative interpolation.

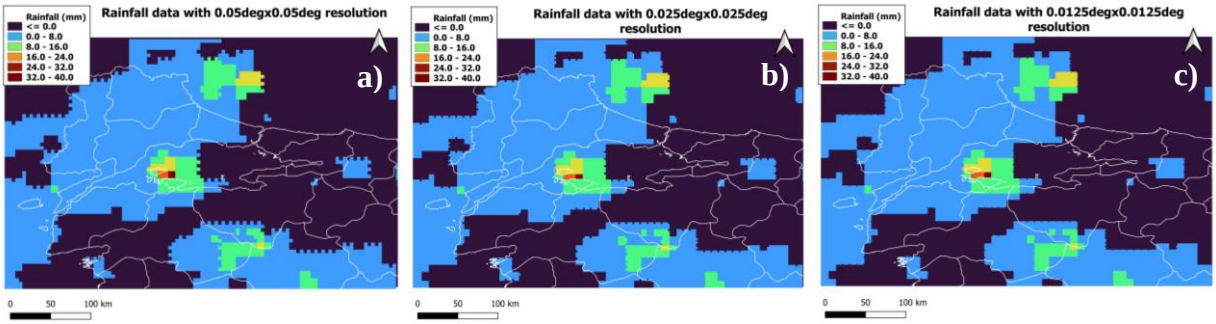

Figure 12. For September 8, 2009, between 11:30-12:00 a.m., (a) Spatially augmented satellite data with 0.05° resolution (x4 higher resolution) (b) Spatially augmented satellite data with 0.025° resolution (x16 higher resolution) (c) Spatially augmented satellite data with 0.0125° resolution (x64 higher resolution) using largest area fraction interpolation.

3.1.1.2. Temporal Data Augmentation

In the temporal augmentation component of the study, the temporal resolution of the rainfall data was increased using linear interpolation, resulting in temporal resolutions of 15, 10 and 5-minute compared to the original temporal resolution of 30-minute as shown in Figure 13-15.

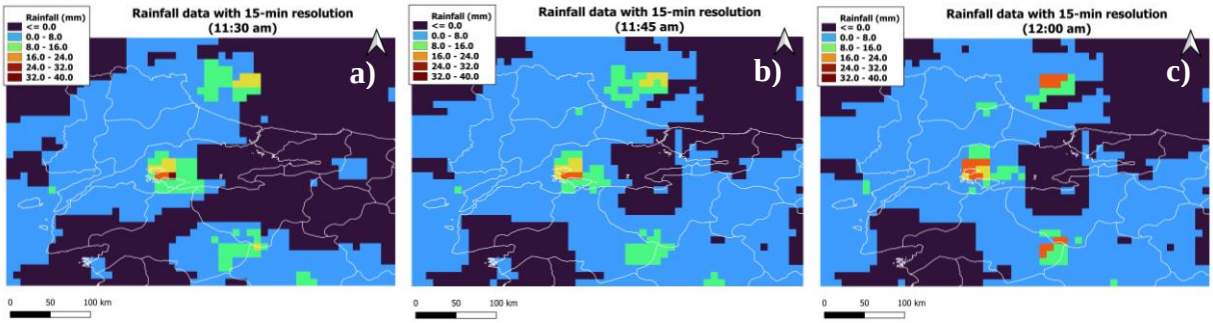

Figure 13. For September 8, 2009, between 11:30-12:00 a.m., temporally augmented satellite data with 15 min resolution using linear interpolation (a) at 11:30 a.m. (b) at 11:45 a.m. (d) at 12:00 a.m.

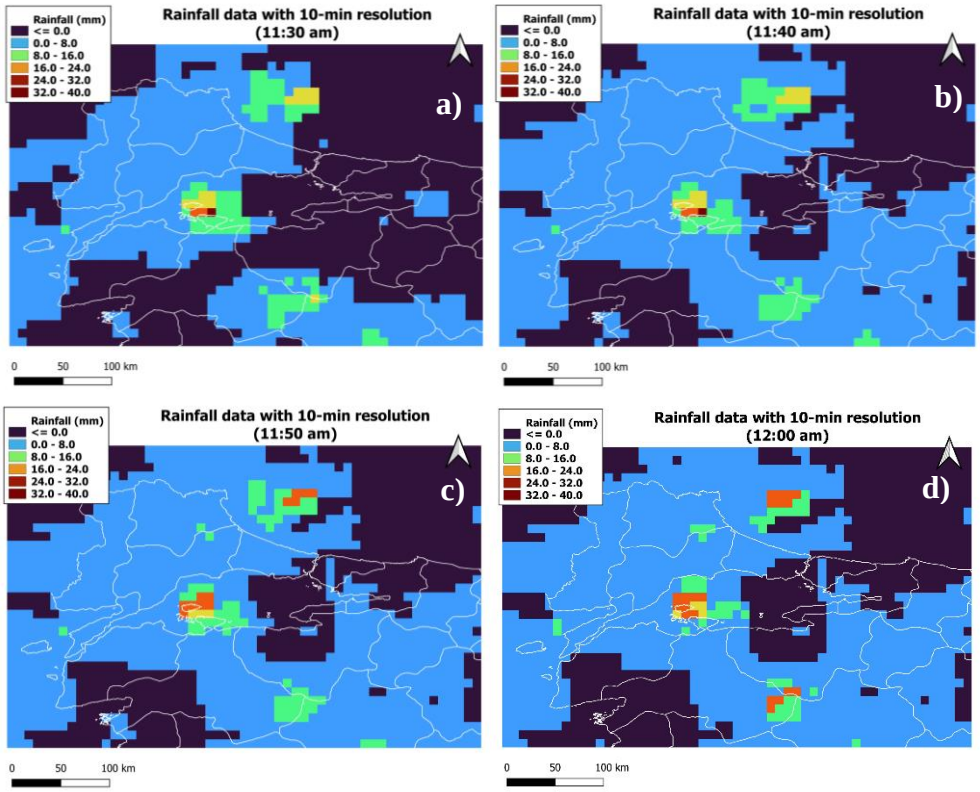

Figure 14. For September 8, 2009, between 11:30-12:00 a.m., temporally augmented satellite data with 10 min resolution (a) at 11:30 a.m. (b) at 11:40 a.m. (c) at 11:50 a.m. (d) at 12:00 a.m.

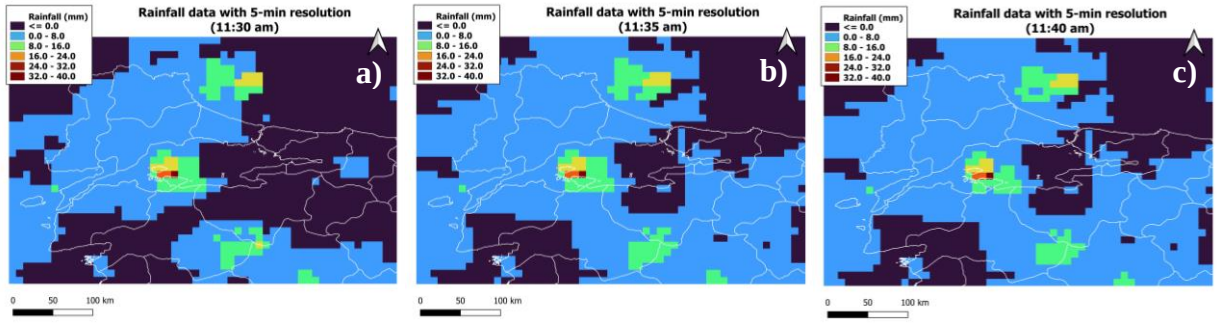

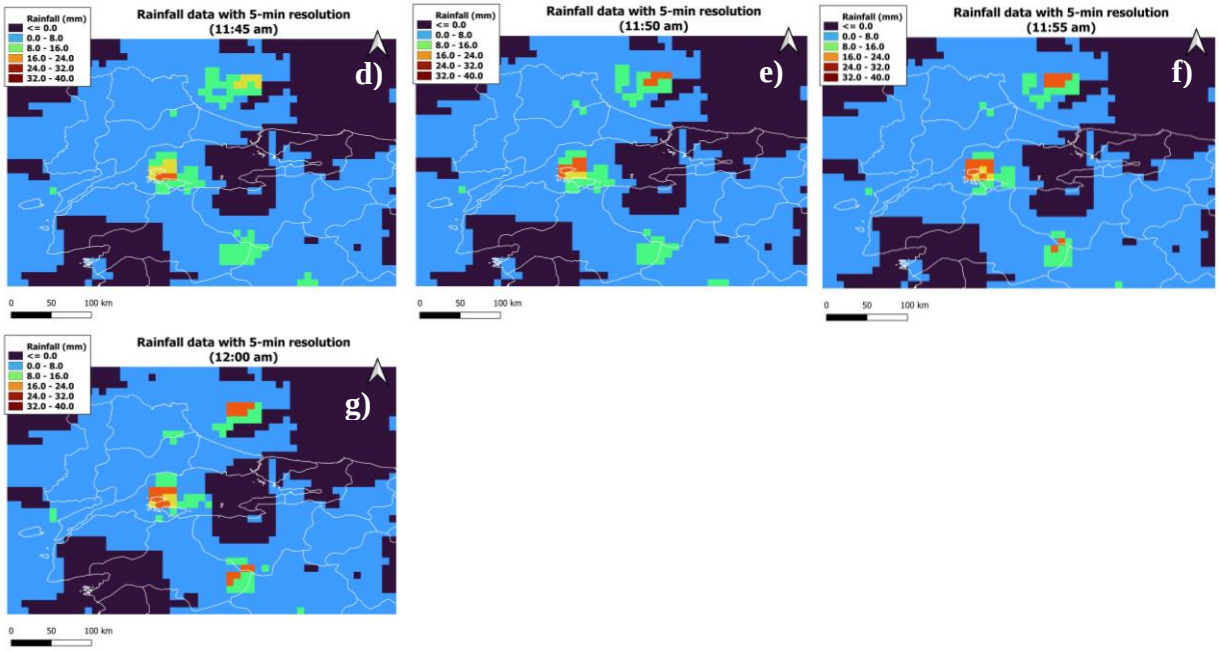

Figure 15. For September 8, 2009, between 11:30-12:00 a.m., temporally augmented satellite data with 5 min resolution (a) at 11:30 a.m. (b) at 11:35 a.m. (c) at 11:40 a.m. (d) at 11:45 a.m. (e) at 11:50 a.m. (f) at 11:55 a.m. (g) at 12:00 a.m.

3.1.1.3. Spatial and Temporal Augmentation

In the section of the study focused on spatiotemporal augmentation, the spatial resolution of the rainfall data was enhanced by factors of 4, 16, and 64 using the aforementioned interpolation methods. Linear interpolation was employed to enhance the temporal resolution of the rainfall data by factors of 2, 3, and 6. Figure 16 presents the most basic spatiotemporally interpolated dataset, featuring a spatial resolution of 0.05° and a temporal resolution of 15 minutes.

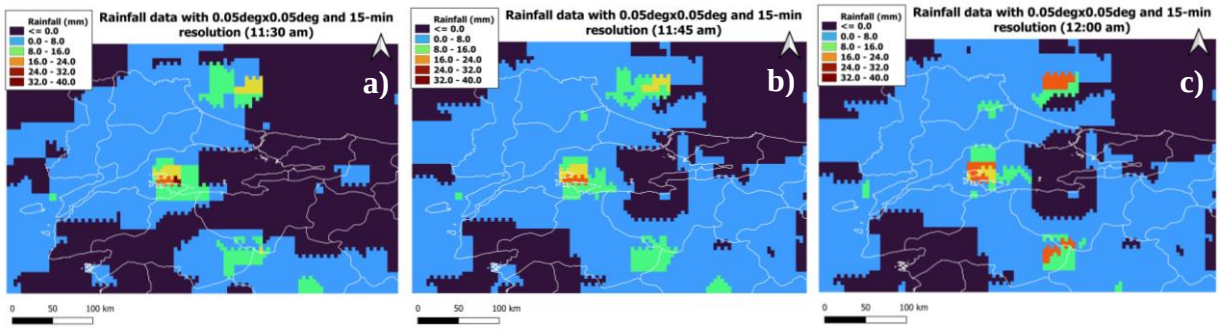

Figure 16. For September 8, 2009, between 11:30-12:00 a.m., either spatially or temporally augmented satellite data with 0.05° spatial resolution and 15 min temporal resolution using nearest neighbor and linear interpolation, respectively (a) at 11:30 a.m. (b) at 11:45 a.m. (d) at 12:00 a.m.

3.1.2. Rainfall Nowcasting

Some nowcasts that involved the utilization of spatially and temporally interpolated data were unable to be executed due to limitations in the available RAM capacity. Additionally, two nowcasts using the data augmented by bilinear and bicubic interpolation did not yield successful outcomes due to the incompatibility between the model and the data. Table 2 presents the outcomes of the conducted nowcast trials.

Table 2. The outcomes of the conducted nowcast trials for both regions.

Spatial interpolation method x Increased Resolution Rate	nnx4	nnx16	nnx64	bilx4	bilx16	bilx64	bicx4	bicx16	bicx64	disx4	disx16	disx64	conx4	conx16	conx64	con2x4	con2x16	con2x64	lafx4	lafx16	lafx64
Feasibleness for Marmara	+	nan	nan	nan	nan	nan	nan	nan	nan	+	nan	nan	+	nan	nan	+	nan	nan	+	nan	nan
Feasibleness for Black Sea	+	nan	nan	nan	nan	nan	nan	nan	nan	+	nan	nan	+	nan	nan	nan	nan	nan	+	nan	nan
Temporal linear interpolation	15 min temporal resolution							10 min temporal resolution							5 min temporal resolution						
Feasibleness for Marmara	+							nan							nan						
Feasibleness for Black Sea	+							nan							nan						
Both spatial and temporal interpolation	nnx4 15m 10m 5m	nnx16 15m 10m 5m	nnx64 15m 10m 5m	bilx4 15m 10m 5m	bilx16 15m 10m 5m	bilx64 15m 10m 5m	bicx4 15m 10m 5m	bicx16 15m 10m 5m	bicx64 15m 10m 5m	disx4 15m 10m 5m	disx16 15m 10m 5m	disx64 15m 10m 5m	conx4 15m 10m 5m	conx16 15m 10m 5m	conx64 15m 10m 5m	con2x4 15m 10m 5m	con2x16 15m 10m 5m	con2x64 15m 10m 5m	lafx4 15m 10m 5m	lafx16 15m 10m 5m	lafx64 15m 10m 5m
Feasibleness for Marmara	nan																				
Feasibleness for Black Sea	nan																				
Interpolation methods	nn: Nearest neighbor interpolation, bil: Bilinear interpolation, bic: Bicubic interpolation, dis: Distance weighted average interpolation, con: first order conservative interpolation, con2: second order conservative interpolation, laf: Largest area fraction interpolation, 15m:15-min linear interpolation, 10m: 10-min linear interpolation, 5-min linear interpolation																				

The investigation commenced by generating a set of 26 distinct datasets comprising both spatially and temporally interpolated data, as well as raw data. At the conclusion of all nowcast experiments, outcomes were derived from nowcasts generated using a mere seven datasets. The reason contributing to the non-completion of 17 out of the remaining 19 studies was the insufficiency of RAM.

Table 3. The hyperparameters that yield optimal outcomes for the Marmara Region flooding.

Hyperparameters	**Best hyperparameter values selected for the Marmara flooding study**
Optimizer	Nadam
Activation function	ReLU
Learning rate	0.0001
Dropout	0.1
Filter numbers	64
Batch size	16, 4*
Batch normalization	✓
Epochs	50

* Due to insufficient RAM capacity in the studies involving all augmented datasets, a nowcast was generated by utilizing a batch size of 4.

As is known, spatiotemporal rainfall data frequently contains a significant number of zero values. When both interpolation and prediction models are applied to points with zero values, it is probable that rainfall values or negative values will be observed at these grids where there is no precipitation. Therefore, the data was standardized and used for this reason as well as for the ease of analysis and comparison. Table 3 displays the optimal hyperparameter configuration for the Marmara Region flooding, which has been determined through a large number of trials. Figure 16 shows training and validation losses for rainfall and augmented rainfall datasets.

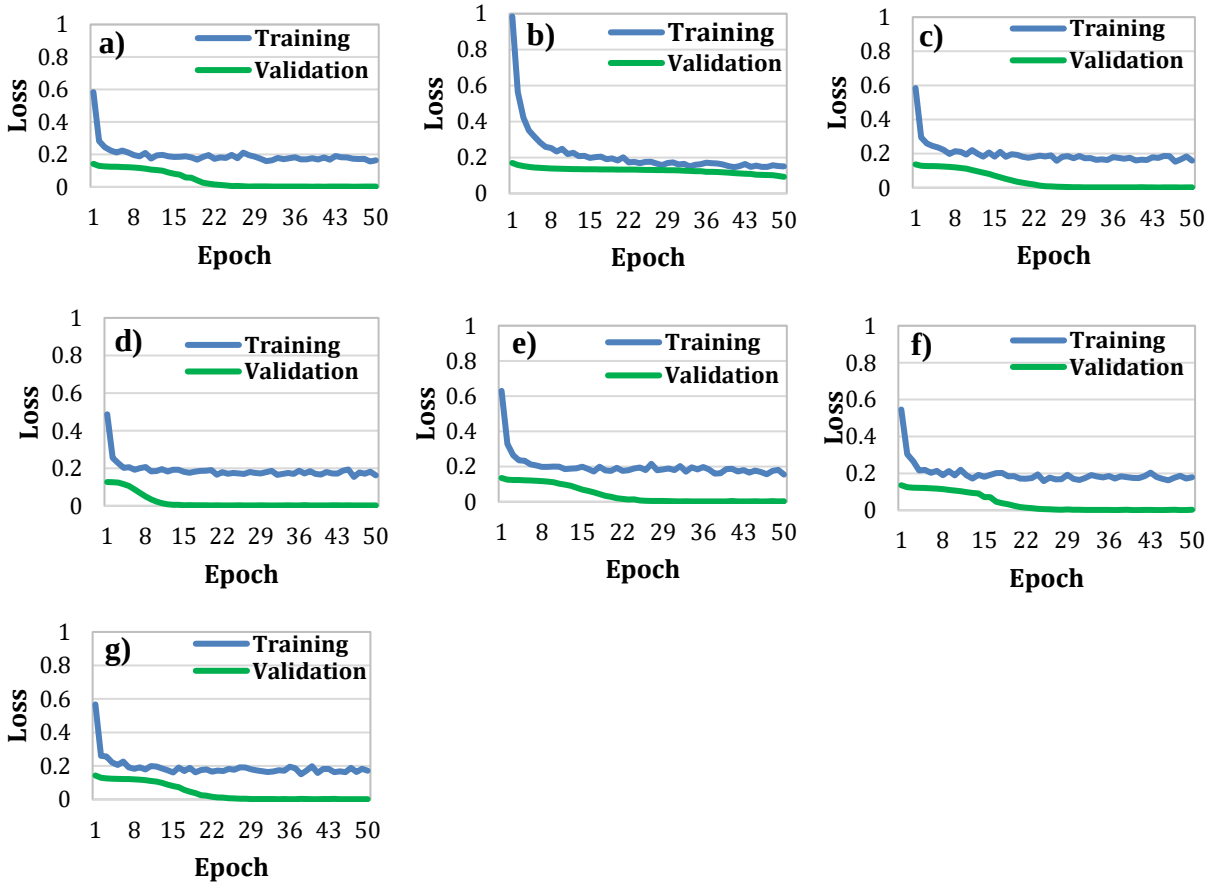

Figure 16. Learning curves of the ConvLSTM model using (a) rainfall data, spatially augmented satellite data with 0.05° resolution using (b) nearest neighbor interpolation (c) distance weighted average interpolation (d) first order conservative interpolation (e) second order conservative interpolation (f) largest area fraction interpolation (g) Temporally augmented satellite data with 15-min resolution using linear interpolation.

As seen in the Figure 16, there are two obvious differences between nowcast with rainfall data and nowcast with augmented data: One notable observation is that the training loss and the validation loss exhibit complete convergence in the nowcast utilizing rainfall data. However, this convergence is not observed in the nowcast employing augmented rainfall datasets. Nevertheless, the error indicators suggest that the predictive accuracy of the nowcast generated using augmented

data is superior. In the present scenario, when considering the nowcast generated using rainfall data, it may be observed that the model exhibits an overfitting to the training data. Specifically, the ConvLSTM model demonstrates a strong ability to learn from the training data but struggles to effectively generalize its findings to unseen data.

The second is convergence speed. The loss in the nowcast with rainfall data starts with a larger value and decreases rapidly. However, the nowcast utilizing augmented rainfall data exhibits a smaller decrease, although the convergence speed is higher and remains constant beyond the 8th epoch. The interpretation of the ConvLSTM model suggests that it is not exhibiting overfitting tendencies towards the training data. In addition, errors of the aforementioned models is comparatively lower than that of the nowcast model incorporating rainfall data. In conclusion, it can be asserted that the utilization of augmented data in nowcast studies leads to enhanced accuracy in predictions. It may be interpreted as meaning that the ConvLSTM model is not overfitting the training data. Moreover, error values are also lower than the nowcast with rainfall data. In conclusion, it can be asserted that the utilization of augmented data in nowcast studies leads to an enhancement in the accuracy of predictions.

In the present investigation, nowcasts were generated for a total of 12 temporal intervals, which corresponded to the preceding 6 hours. Figure 17 displays a series of frames with the standardized data representing the last 12 time periods for the Marmara Region.

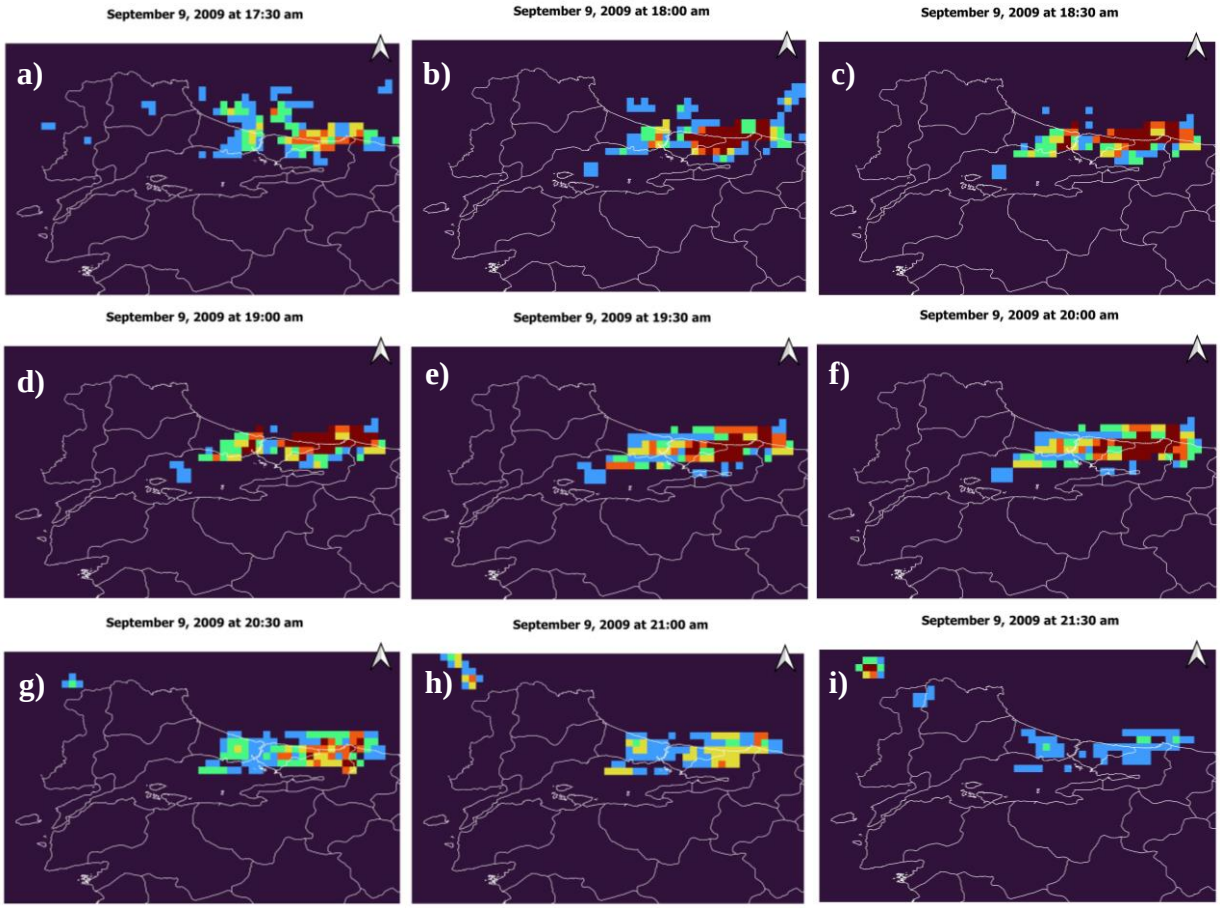

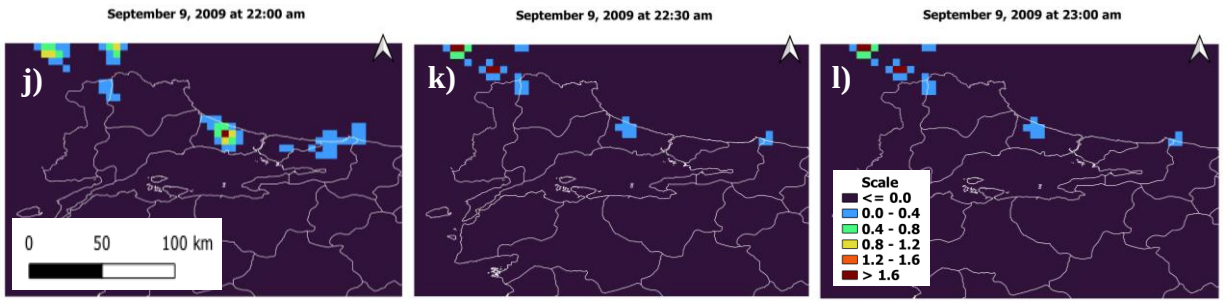

Figure 17. The last consecutive 12 frames for Marmara Region nowcast. For September 9, 2009 (a) 17:30 a.m. (b) 18:00 a.m. (c) 18:30 a.m. (d) 19:00 a.m. (e) 19:30 a.m. (f) 20:00 a.m. (g) 20:30 a.m. (h) 21:00 a.m. (i) 21:30 a.m. (j) 22:00 a.m. (k) 22:30 a.m. (l) 23:00 a.m.

Upon analyzing the preceding 12 frames, it becomes evident that the conclusion of the flood is imminent and there has been a significant reduction in rainfall. The nowcast results for each dataset at 17:30 a.m. are presented in Figure 18.

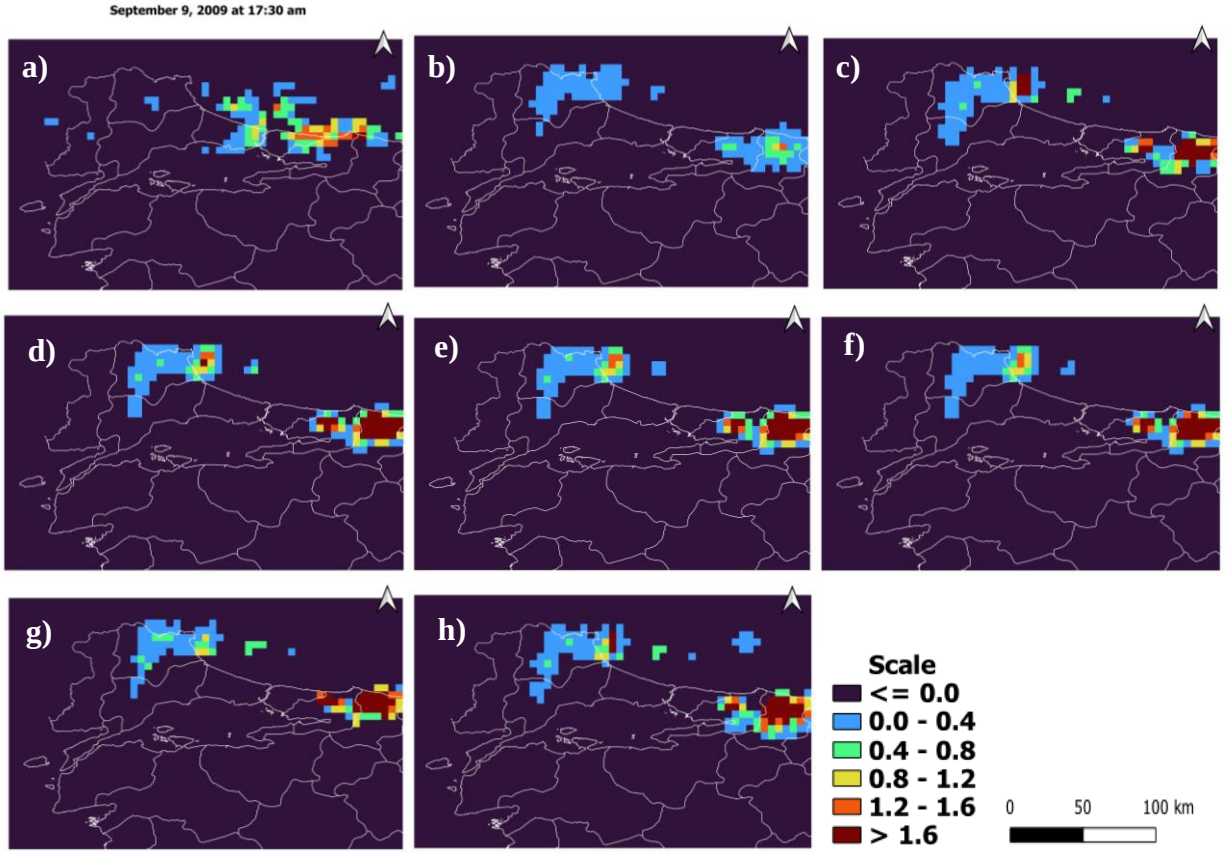

Figure 18. (a) Rainfall data, nowcast results for September 9, 2009, at 20:00 a.m. using (b) rainfall data, spatially augmented rainfall data via (c) nearest neighbor interpolation (d) distance weighted average interpolation (e) first order conservative interpolation (f) second order conservative interpolation (g) largest area fraction interpolation (h) temporally augmented rainfall data via linear interpolation.

Upon examination of the nowcast outcomes presented in Figure 18, it becomes evident that the model exhibits a greater degree of predictive accuracy in areas characterized by substantial precipitation as compared to regions with minimal rainfall. This study employed root mean square error (RMSE) and mean absolute error (MAE) as performance criteria, consistent with previous studies (Kumar et al., 2020; Gad et al., 2021; Amini et al., 2022) that utilized these metrics. The error values for the nowcasts are presented in Table 4. According to the findings presented in Table 4, the implementation of data augmentation techniques has been observed to enhance the accuracy of nowcasting. Based on the data presented in the table, it can be observed that the RMSE and MAE values exhibited a reduction of up to 59% when employing augmented data in the nowcast. In all nowcasts generated using augmented data, the error values exhibit a high degree of similarity. There is a lack of substantial disparity in the level of success observed among various interpolation methods.

Table 4. The error values for the nowcasts.

Datasets	**RMSE**	**MAE**
Rainfall data	0.2966	0.2786
Spatially augmented satellite data with 0.05° resolution using nearest neighbor interpolation	0.1853	0.1373
Spatially augmented satellite data with 0.05° resolution using distance weighted average interpolation	0.1759	0.1248
Spatially augmented satellite data with 0.05° resolution using first order conservative interpolation	0.1762	0.1269
Spatially augmented satellite data with 0.05° resolution using second order conservative interpolation	0.1739	0.1251
Spatially augmented satellite data with 0.05° resolution using largest area fraction interpolation	0.1792	0.1305
Temporally augmented satellite data with 15-min resolution using linear interpolation	0.1901	0.1445

3.2. Central Black Sea Region

The Black Sea Region is characterized by being the recipient of the highest amount of rainfall. The Central Black Sea region exhibits the lowest precipitation levels in comparison to its western and eastern counterparts. Notwithstanding this, the duration of the flood spanning five days resulted in significant destruction owing to the geographical alignment of the mountains in this area running parallel to the coastline, coupled with inadequate urban development practices in the beds of the watercourses. In a manner akin to the research undertaken for the Marmara Region, the present study involved the generation of nowcasts using both raw and augmented data, followed by an analysis of the resultant nowcast outcomes.

3.2.1. Data Augmentation

3.2.1.1. Spatial Data Augmentation

Figure 19 presents the rainfall data observed during the time interval from 10:00 to 10:30 a.m. on August 11, 2021. The spatial resolution of the rainfall data provided is 0.1° x 0.1°. In the spatial augmentation component of the investigation, the spatial resolution of the rainfall data was increased via interpolation methods, resulting in a spatial resolution of 0.5°x0.5°, 0.025°x0.025° and 0.0125°x0.0125° (see Fig. 20-26).

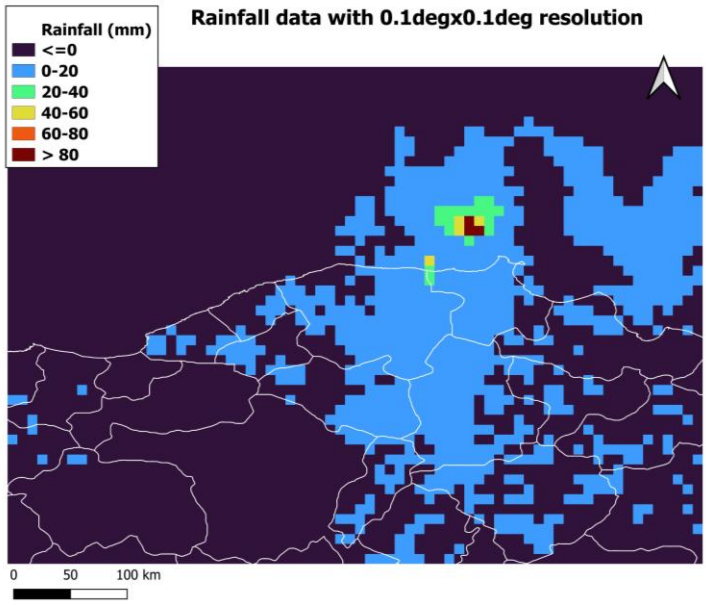

Figure 19. For August 11, 2021, between 10:30-11:00 a.m., rainfall data with 0.1°x0.1° spatial resolution.

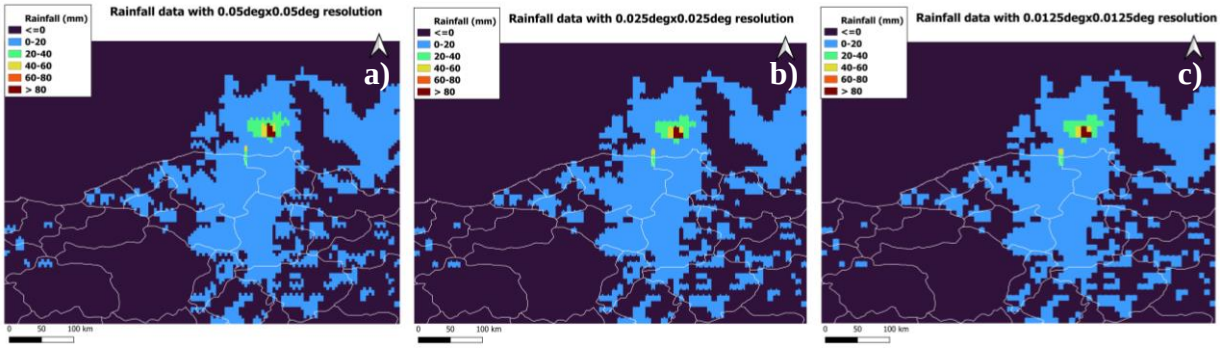

Figure 20. For August 11, 2021, between 10:30-11:00 a.m., (a) Spatially augmented satellite data with 0.05° resolution (x4 higher resolution) (b) Spatially augmented satellite data with 0.025° resolution (x16 higher resolution) (c) Spatially augmented satellite data with 0.0125° resolution (x64 higher resolution) using nearest neighbor interpolation.

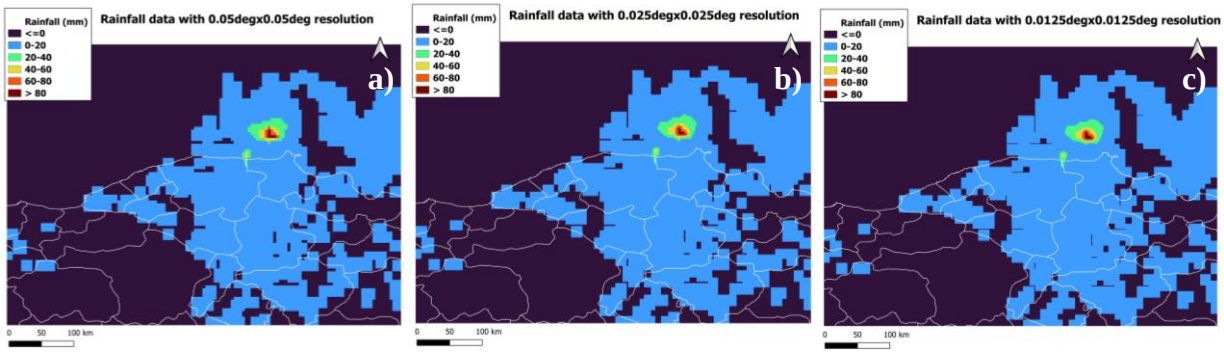

Figure 21. For August 11, 2021, between 10:30-11:00 a.m., (a) Spatially augmented satellite data with 0.05° resolution (x4 higher resolution) (b) Spatially augmented satellite data with 0.025° resolution (x16 higher resolution) (c) Spatially augmented satellite data with 0.0125° resolution (x64 higher resolution) using bilinear interpolation.

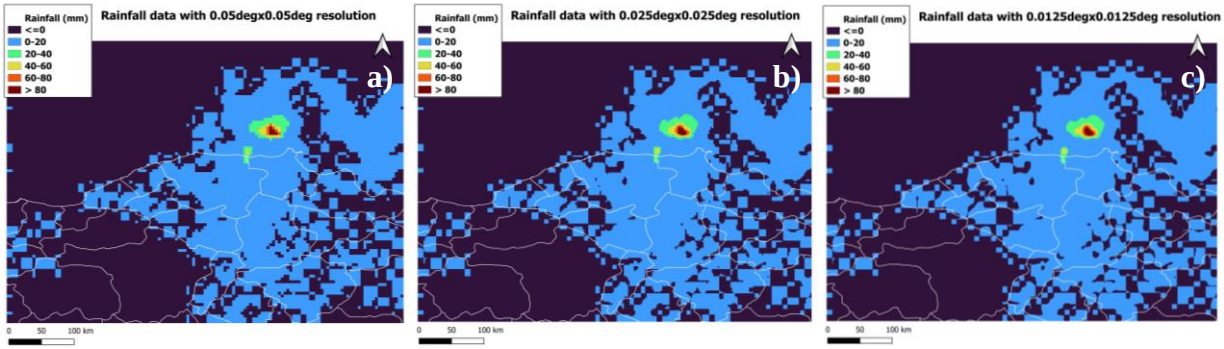

Figure 22. For August 11, 2021, between 10:30-11:00 a.m., (a) Spatially augmented satellite data with 0.05° resolution (x4 higher resolution) (b) Spatially augmented satellite data with 0.025° resolution (x16 higher resolution) (c) Spatially augmented satellite data with 0.0125° resolution (x64 higher resolution) using bicubic interpolation.

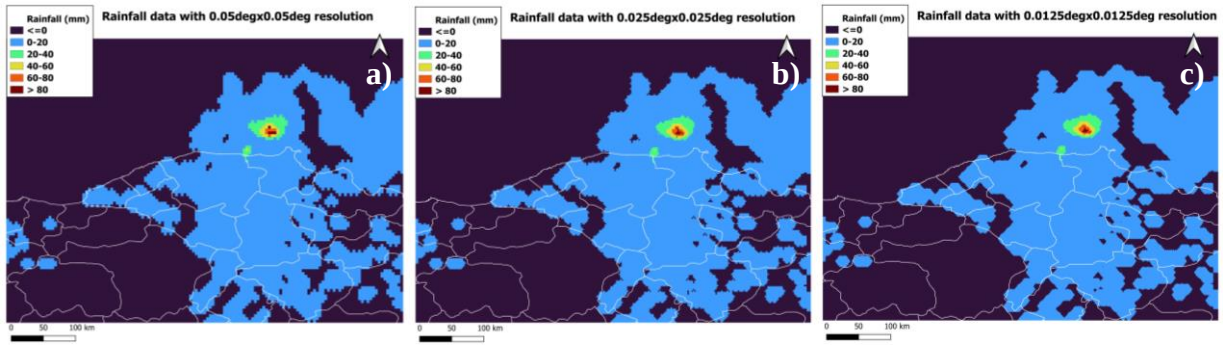

Figure 23. For August 11, 2021, between 10:30-11:00 a.m., (a) Spatially augmented satellite data with 0.05° resolution (x4 higher resolution) (b) Spatially augmented satellite data with 0.025° resolution (x16 higher resolution) (c) Spatially augmented satellite data with 0.0125° resolution (x64 higher resolution) using distance weighted average interpolation.

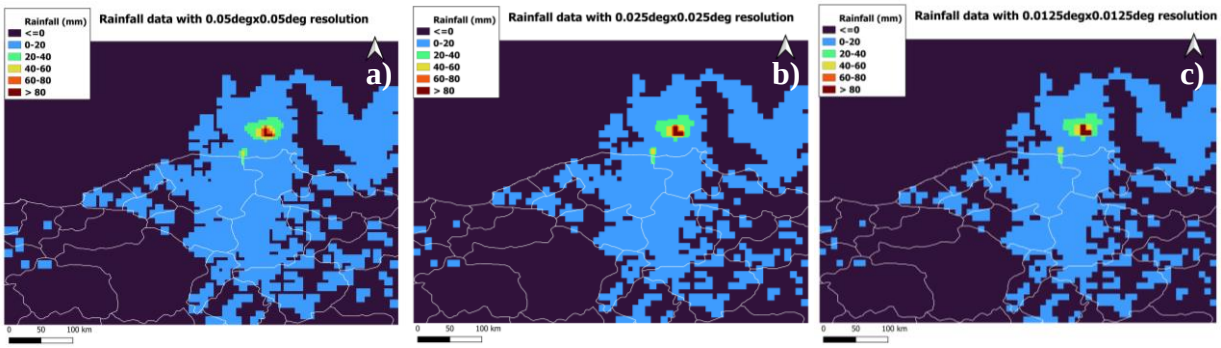

Figure 24. For August 11, 2021, between 10:30-11:00 a.m., a) Spatially augmented satellite data with 0.05° resolution (x4 higher resolution) (b) Spatially augmented satellite data with 0.025° resolution (x16 higher resolution) (c) Spatially augmented satellite data with 0.01250 resolution (x64 higher resolution) using first order conservative interpolation.

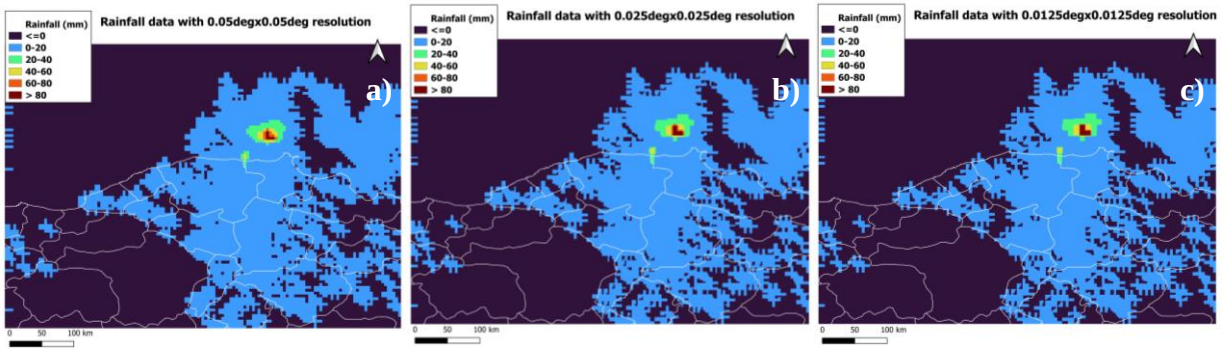

Figure 25. For August 11, 2021, between 10:30-11:00 a.m., (a) Spatially augmented satellite data with 0.05° resolution (x4 higher resolution) (b) Spatially augmented satellite data with 0.025° resolution (x16 higher resolution) (c) Spatially augmented satellite data with 0.0125° resolution (x64 higher resolution) using second order conservative interpolation.

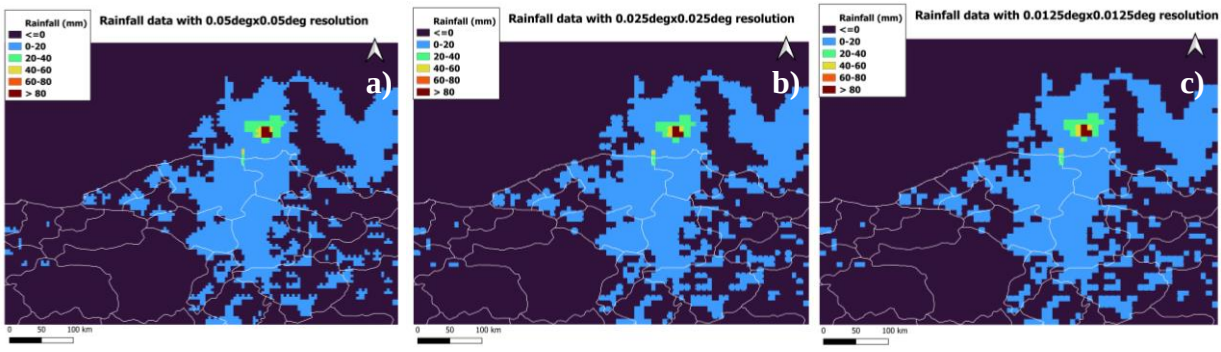

Figure 26. For August 11, 2021, between 10:30-11:00 a.m., (a) Spatially augmented satellite data with 0.05° resolution (x4 higher resolution) (b) Spatially augmented satellite data with 0.025° resolution (x16 higher resolution) (c) Spatially augmented satellite data with 0.0125° resolution (x64 higher resolution) using largest area fraction interpolation.

3.2.1.2. Temporal Data Augmentation

In the temporal augmentation component of the investigation, the temporal resolution of the rainfall data was increased using linear interpolation, resulting in temporal resolutions of 15, 10 and 5-minute compared to the original temporal resolution of 30-minute as shown in Figure 27-29.

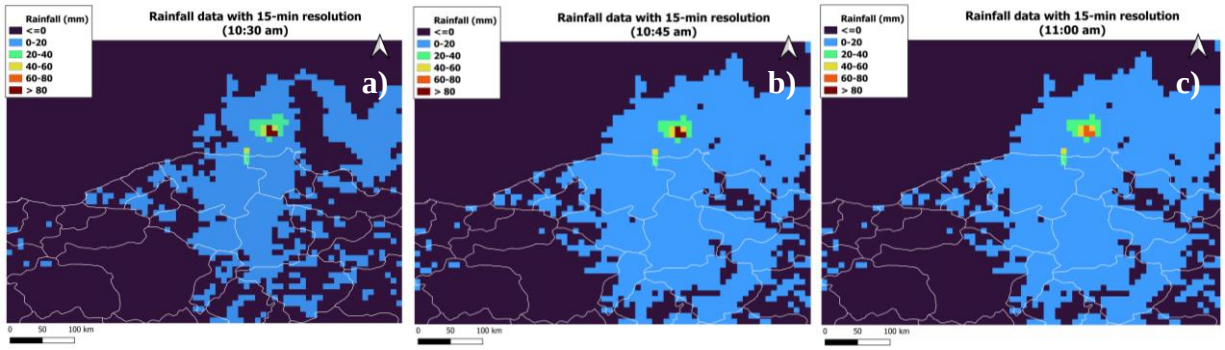

Figure 27. For August 11, 2021, between 10:30-11:00 a.m., temporally augmented satellite data with 15 min resolution using linear interpolation (a) at 10:30 a.m. (b) at 10:45 a.m. (d) at 11:00 a.m.

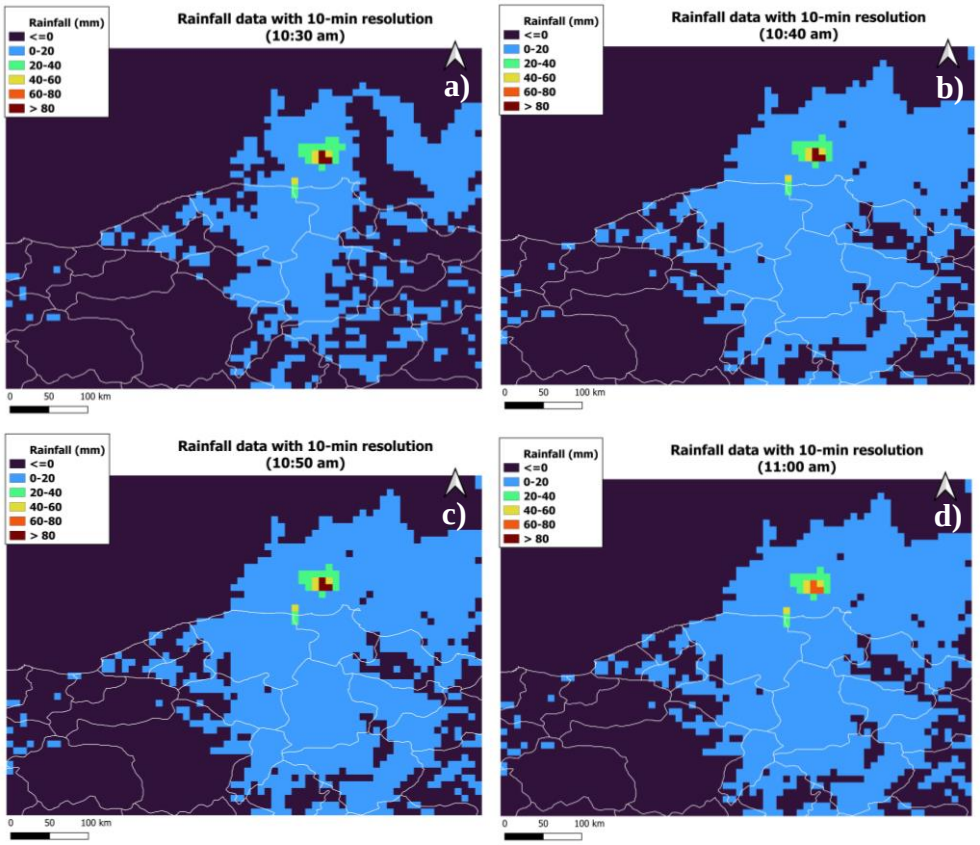

Figure 28. For August 11, 2021, between 10:30-11:00 a.m., temporally augmented satellite data with 10 min resolution (a) at 10:30 a.m. (b) at 10:40 a.m. (c) at 10:50 a.m. (d) at 11:00 a.m.

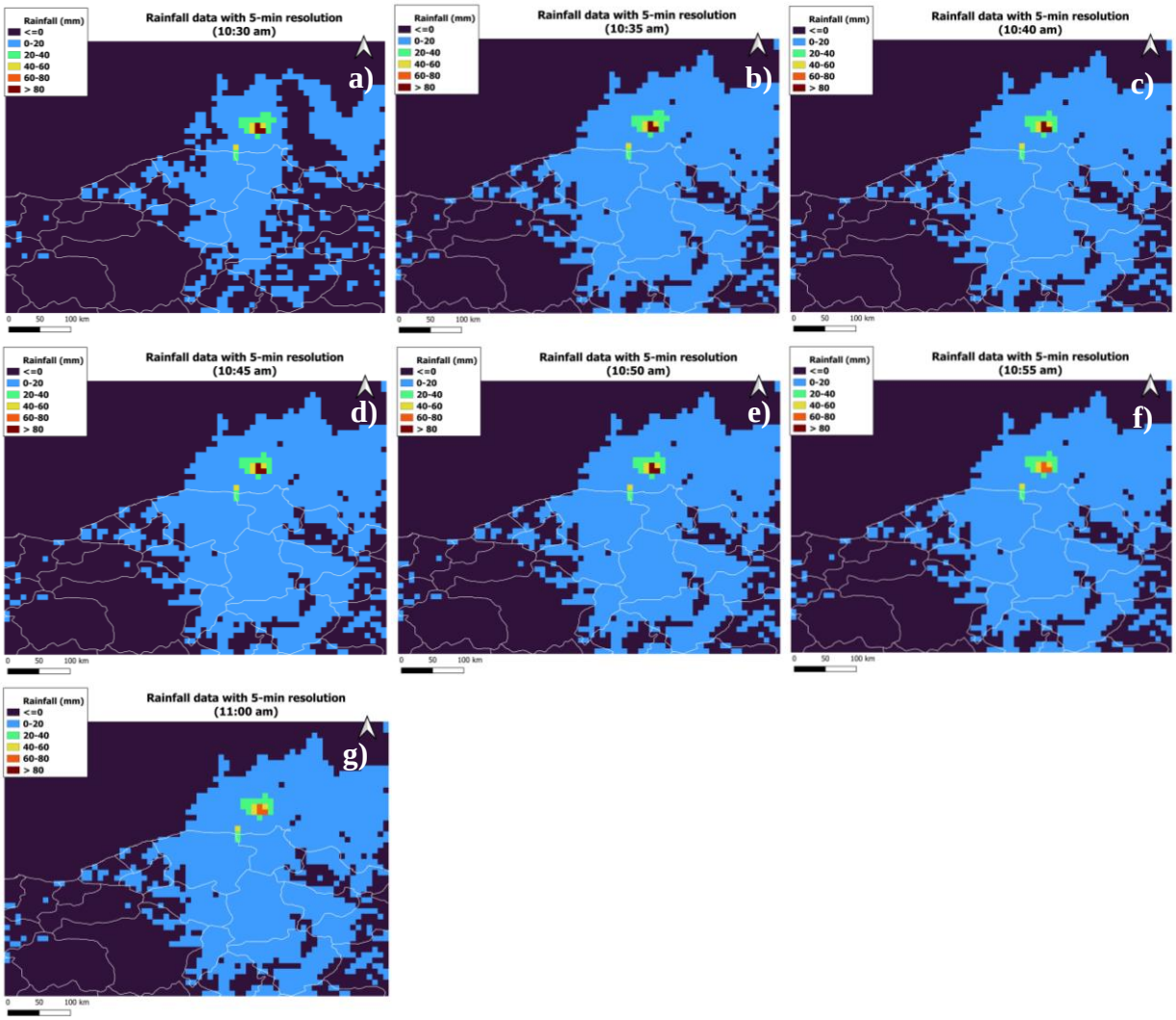

Figure 29. For August 11, 2021, between 10:30-11:00 a.m., temporally augmented satellite data with 5 min resolution (a) at 10:30 a.m. (b) at 10:35 a.m. (c) at 10:40 a.m. (d) at 10:45 a.m. (e) at 10:50 a.m. (f) at 10:55 a.m. (g) at 11:00 a.m.

3.2.1.3. Spatial and Temporal Augmentation

Linear interpolation increased rainfall data temporal resolution by 2, 3, and 6. Figure 30 shows the spatiotemporally interpolated dataset, with 0.05° spatial resolution and 15 minutes temporal resolution.

3.2.2. Rainfall Nowcasting

Table 5 presents the optimal hyperparameter configuration for the Central Black Region flooding, which has been derived from an extensive series of trials.

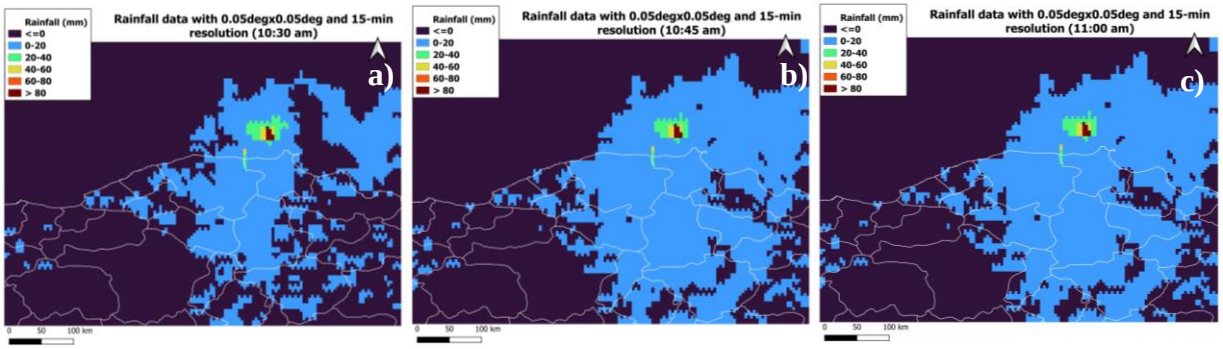

Figure 30. For August 11, 2021, between 10:30-11:00 a.m., either spatially or temporally augmented satellite data with 0.05° spatial resolution and 15 min temporal resolution using nearest neighbor and linear interpolation, respectively (a) at 10:30 a.m. (b) at 10:45 a.m. (d) at 11:00 a.m.

Table 5. The hyperparameters that yield optimal outcomes for the Central Black Sea Region flooding.

Hyperparameters	**Best hyperparameter values for the Marmara flooding study**
Optimizer	Adam
Activation function	ReLU
Learning rate	0.0001
Dropout	0.1
Filter numbers	64
Batch size	4, 2*
Batch normalization	✓

* In studies that utilized augmented datasets, nowcasts were generated by utilizing a batch size of 2, as this was necessary due to the constraints imposed by limited RAM capacity.

Figure 31 displays the training and validation losses pertaining to both the rainfall dataset and the augmented rainfall dataset. From Figure 31, the training loss and the validation loss do not exhibit convergence fully in all nowcasts. While there is a small improvement in the loss values observed when comparing nowcasts generated using raw data versus augmented data, the magnitude of this improvement is insufficient to significantly influence the accuracy of the nowcast. The primary distinction of significance between nowcasting utilizing rainfall data and nowcasting via augmented data lies in the speed of convergence. The analysis reveals that the speed of convergence in nowcasting significantly increases when augmented data is incorporated, exhibiting a nearly twofold acceleration. Furthermore, the speed at which the nowcast converges is significantly higher when temporally augmented data is utilized compared to other forms of augmented data.

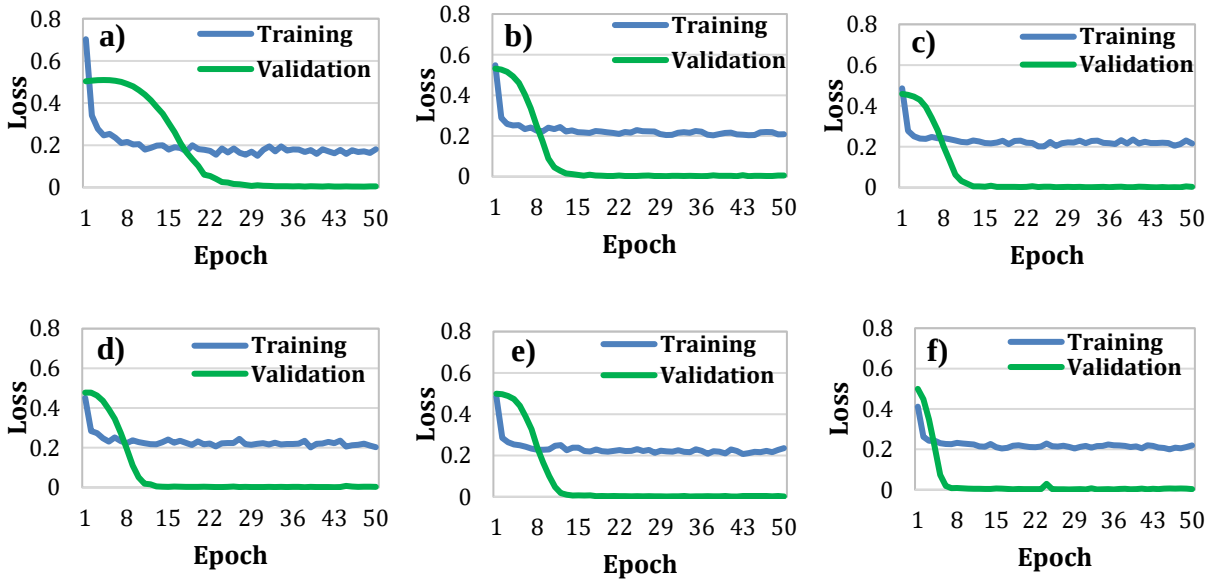

Figure 31. Learning curves of the ConvLSTM model using (a) rainfall data, spatially augmented satellite data with 0.05° resolution using (b) nearest neighbor interpolation (c) distance weighted average interpolation (d) first order conservative interpolation (e) largest area fraction interpolation (f) Temporally augmented satellite data with 15-min resolution using linear interpolation.

In this study, nowcasts were employed for a total of 12 temporal intervals, which represented 6 hours. Figure 32 presents a sequence of frames containing standardized data that represents the most recent 12 time periods for the Central Black Sea Region. The results of the nowcast for each dataset at 19:30 a.m. are depicted in Figure 33.

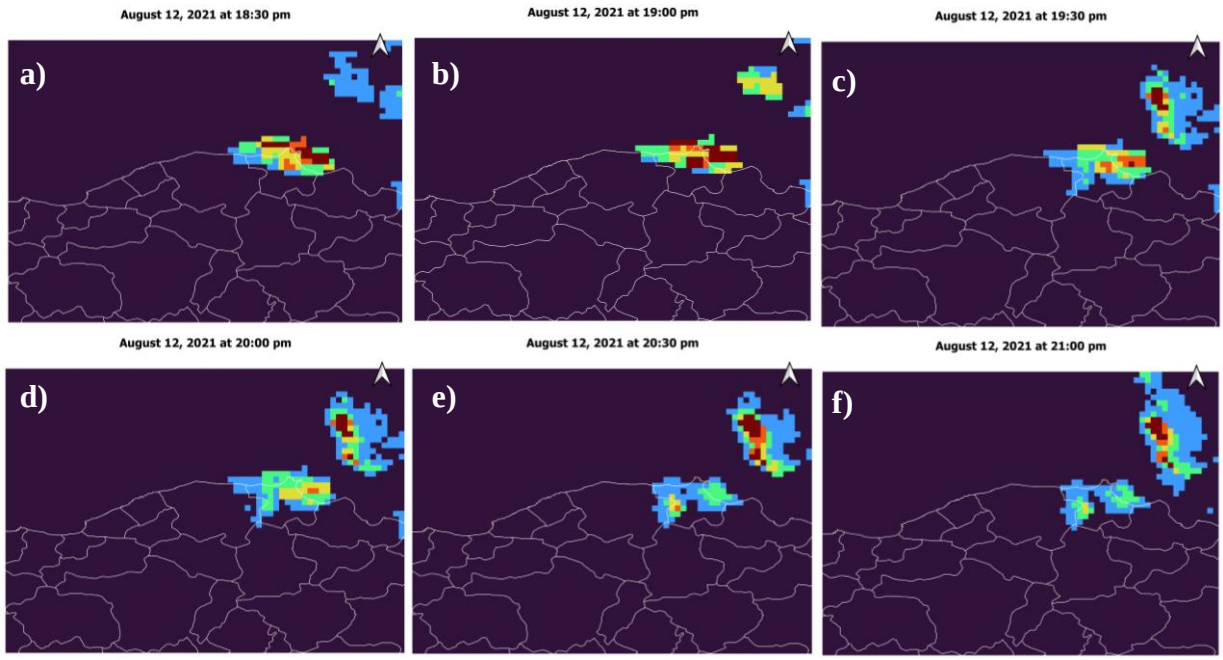

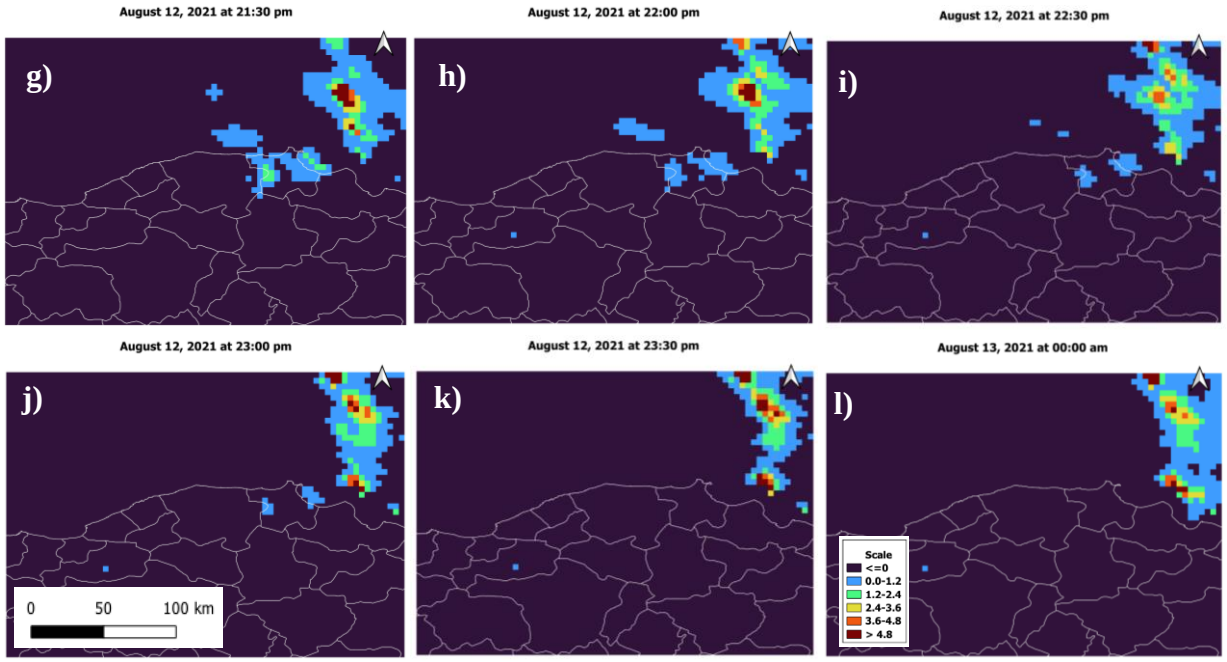

Figure 32. The last consecutive 12 frames for Central Black Sea Region nowcast. For August 12, 2021 (a) 18:30 p.m. (b) 19:00 p.m. (c) 19:30 p.m. (d) 20:00 p.m. (e) 20:30 p.m. (f) 21:00 p.m. (g) 21:30 p.m. (h) 22:00 p.m. (i) 22:30 p.m. (j) 23:00 p.m. (k) 23:30 p.m. (l) August 13, 2021, 00:00 a.m.

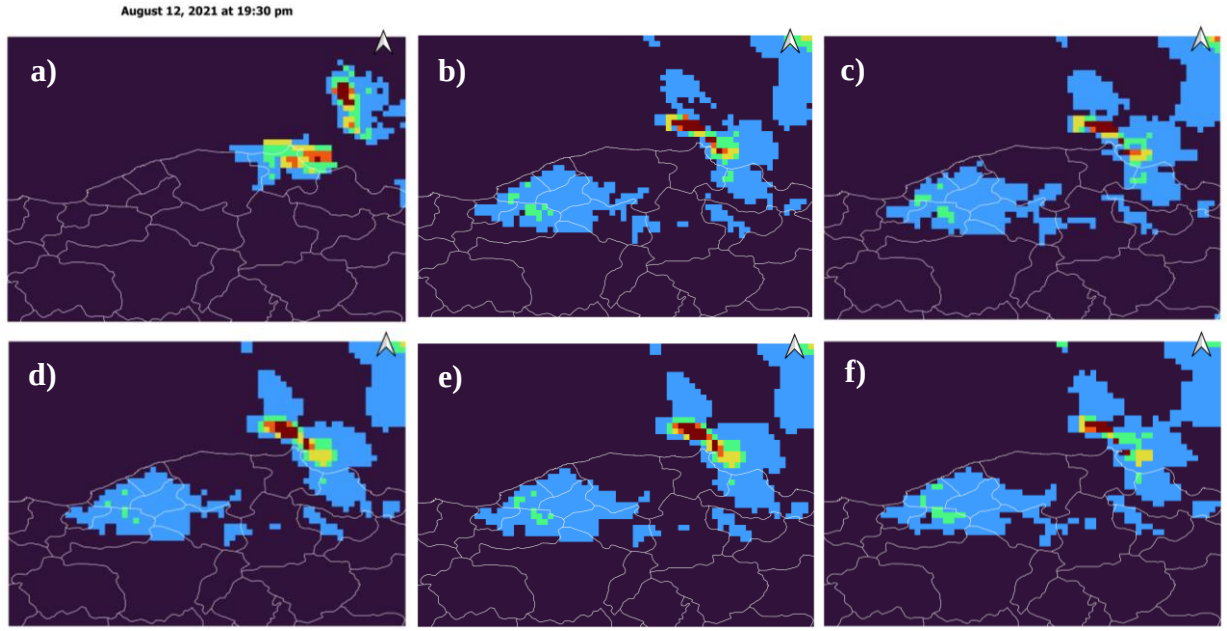

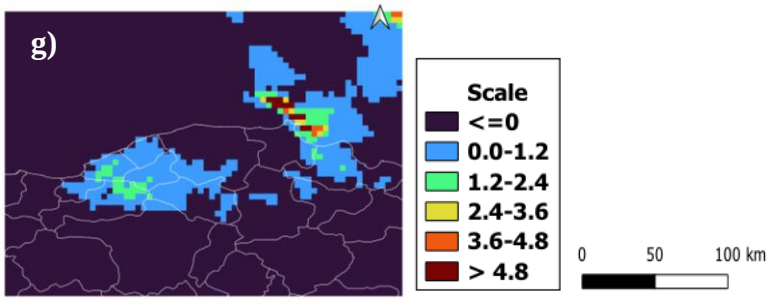

Figure 33. (a) Rainfall data, nowcast results for August 12, 2021, at 19:30 a.m. using (b) rainfall data, spatially augmented rainfall data via (c) nearest neighbor interpolation (d) distance weighted average interpolation (e) first order conservative interpolation (f) largest area fraction interpolation (g) temporally augmented rainfall data via linear interpolation.

According to Figure 33, it can be said that the ConvLSTM model's ability to accurately nowcast flooding in the Black Sea region is lower when compared to its performance in the Marmara region. The error values for the nowcasts are presented in Table 6. The analysis of Table 6 reveals that the incorporation of augmented data did not yield any discernible impact on the error values of the nowcast.

Table 6. The error values for the nowcasts models.

Datasets	**RMSE**	**MAE**
Rainfall data	0.2789	0.2011
Spatially augmented satellite data with 0.05° resolution using nearest neighbor interpolation	0.2784	0.2033
Spatially augmented satellite data with 0.05° resolution using distance weighted average interpolation	0.2681	0.1965
Spatially augmented satellite data with 0.05° resolution using first order conservative interpolation	0.2740	0.2027
Spatially augmented satellite data with 0.05° resolution using largest area fraction interpolation	0.2850	0.2050
Temporally augmented satellite data with 15-min resolution using linear interpolation	0.2801	0.2058

4. Conclusion

The task of predicting rainfall in real-time is challenging due to the intricate and ever-changing characteristics of atmospheric phenomena. Numerous research endeavors are currently underway to enhance the accuracy of prediction through the utilization of physical models as well as novel artificial intelligence techniques. However, the escalating frequency of flash floods and severe flooding events, attributed to the effects of climate change, amplifies the significance of this and comparable research endeavors.

This study involved the development of a rainfall nowcast model utilizing a deep learning methodology. The nowcast was subsequently conducted for two distinct flood scenarios, each utilizing distinct datasets which are rainfall data derived from the NASA Giovanni satellite and augmented versions of this data. The primary objective of this study was to ascertain the feasibility of establishing a general rule through a comparative analysis of nowcasts generated using original data and augmented data using deep learning.

The primary challenge encountered during the study pertained to the insufficiency of hardware resources when executing the model on a laptop computer. Despite the utilization of a simple ConvLSTM model and Google Colab Pro+, numerous attempts were made to generate nowcasts using various datasets, necessitating extensive waiting periods for the computation of results.

The Marmara and Black Sea regions exhibit notable disparities in terms of topography, synoptic patterns, and local orographic characteristics. Due to this factor, precipitation patterns exhibit significant variations across different regions. Hence, these two distinct flood occurrences were selected as case studies to ensure their representativeness.

The quantity of data points plays a crucial role in deep learning methodologies as it enhances the model's ability to effectively learn from the provided data. From this particular standpoint, a total of eight distinct interpolation techniques were employed in order to enhance the resolution of the data in terms of both spatial and temporal dimensions. When examining data augmentation experiments, it is clearly seen that the utilization of bilinear and first-order conservative interpolation techniques makes interpolating the data more feasible for both regions.

Following the completion of the data augmentation phase in the study, a comprehensive evaluation of the hyperparameters listed in Table 1 was conducted. Through this evaluation, the hyperparameters that yielded the most accurate nowcast result were identified. The notable observation at this juncture is that different optimizers yielded superior outcomes, despite employing the identical model and utilizing the same type of data (i.e., satellite-derived precipitation products).

The concluding stage of the study involves generating 6-hour nowcasts for 12 temporal intervals, utilizing the hyperparameters that have been determined. The same model was executed using the most suitable hyperparameters for two distinct regions. In the investigation of optimal hyperparameters, it was observed that the rainfall nowcast outcomes exhibited variations across two distinct geographical regions. In the present study, the application of augmented data in nowcast models resulted in a significant reduction of error values in rainfall nowcasts within the Marmara Region. Specifically, the error values were observed to decrease by 50%. Conversely, the utilization of augmented data in nowcast models within the Central Black Sea Region did not yield any discernible impact on the accuracy of the forecasts. Due to the presence of the North Anatolian Mountains, which span across the Black Sea Region in an east-west orientation, orographic precipitation occurs, resulting in substantial levels of precipitation in this area. This study has demonstrated once more that individual rainfall and flood events possess distinct characteristics, including unique structural attributes, synoptic factors, and local features. It is important to note that a model that demonstrates efficacy in accurately predicting a specific rainfall

event may not necessarily yield comparable results when applied to another rainfall nowcast. Furthermore, the incorporation of augmented data may not consistently prove useful in every flood event nowcast.

The utilization of numerical weather models presents specific challenges, including computational costs and time consumption. Therefore, using machine learning algorithms and, even better, combining conventional methods with machine learning algorithms may prove advantageous in addressing these issues. In order to enhance the scope of this study, it may be advantageous to ascertain the specific type of rainfall, namely orographic, cyclonic, or conventional, and subsequently develop a more intricate model with using high-performance computing.

5. Acknowledgement

The funding for this study was provided by the Scientific and Technological Research Institution of Türkiye (TÜBİTAK), specifically through the 2219 International Postdoctoral Fellowship Program, under Grant Number 1059B191900568.

6. References

Adaryani, F. R., Mousavi, S. J., & Jafari, F. (2022). Short-term rainfall forecasting using machine learning-based approaches of PSO-SVR, LSTM and CNN. *Journal of Hydrology*, *614*, 128463.

Alabbad, Y., & Demir, I. (2022). Comprehensive flood vulnerability analysis in urban communities: Iowa case study. International journal of disaster risk reduction, 74, 102955.

Amini, A., Dolatshahi, M., & Kerachian, R. (2022). Adaptive precipitation nowcasting using deep learning and ensemble modeling. *Journal of Hydrology*, *612*, 128197.

Amini, A., Dolatshahi, M., & Kerachian, R. (2023). Effects of Automatic Hyperparameter Tuning on the Performance of Multi-variate Deep Learning-based Rainfall Nowcasting. *Water Resources Research*, e2022WR032789.

Bayar, S., Demir, I., & Engin, G. O. (2009). Modeling leaching behavior of solidified wastes using back-propagation neural networks. Ecotoxicology and environmental safety, 72(3), 843-850.

Baydaroğlu, Ö., & Koçak, K. (2014). SVR-based prediction of evaporation combined with chaotic approach. *Journal of Hydrology*, *508*, 356-363.

Beck, M.B., Jiang, F., Shi, F., Walker, R.V., Osidele, O.O., Lin, Z., Demir, I. and Hall, J.W., (2010), March. Re-engineering cities as forces for good in the environment. In Proceedings of the Institution of Civil Engineers-Engineering Sustainability (Vol. 163, No. 1, pp. 31-46). Thomas Telford Ltd.

Burrough, P. A., McDonnell, R. A., & Lloyd, C. D. (2015). *Principles of geographical information systems*. Oxford University Press.

Chen, H., Sheng, S., Xu, C. Y., Li, Z., Zhang, W., Wang, S., & Guo, S. (2021). A spatiotemporal estimation method for hourly rainfall based on F-SVD in the recommender system. *Environmental Modelling & Software*, *144*, 105148.

Chen, C., Zhang, Q., Kashani, M. H., Jun, C., Bateni, S. M., Band, S. S., ... & Chau, K. W. (2022). Forecast of rainfall distribution based on fixed sliding window long short-term memory. *Engineering Applications of Computational Fluid Mechanics*, *16*(1), 248-261.

Chen, S., Xu, X., Zhang, Y., Shao, D., Zhang, S., & Zeng, M. (2022). Two-stream convolutional LSTM for precipitation nowcasting. *Neural Computing and Applications*, *34*(16), 13281-13290.

Chen, C., Jiang, J., Liao, Z., Zhou, Y., Wang, H., & Pei, Q. (2022). A short-term flood prediction based on spatial deep learning network: A case study for Xi County, China. *Journal of Hydrology*, *607*, 127535.

Collins, F. C. (1995). *A comparison of spatial interpolation techniques in temperature estimation* (Doctoral dissertation, Virginia Tech).

Demiray, B. Z., Sit, M., & Demir, I. (2021). DEM super-resolution with efficientNetV2. arXiv preprint arXiv:2109.09661.

Demiray, B. Z., Sit, M., & Demir, I. (2023). EfficientTempNet: Temporal Super-Resolution of Radar Rainfall. arXiv preprint arXiv:2303.05552.

Deo, R. C., Byun, H. R., Adamowski, J. F., & Kim, D. W. (2015). A real-time flood monitoring index based on daily effective precipitation and its application to Brisbane and Lockyer Valley flood events. *Water Resources Management*, *29*, 4075-4093.

Gad, I., Hosahalli, D., Manjunatha, B. R., & Ghoneim, O. A. (2021). A robust deep learning model for missing value imputation in big NCDC dataset. *Iran Journal of Computer Science*, *4*, 67-84.

Halgamuge, M. N., Daminda, E., & Nirmalathas, A. (2020). Best optimizer selection for predicting bushfire occurrences using deep learning. *Natural Hazards*, *103*(1), 845-860.

Islam, S. S., Yeşilköy, S., Baydaroğlu, Ö., Yildirim, E., & Demir, I. (2023). State-Level Multidimensional Agricultural Drought Susceptibility and Risk Assessment for Agriculturally Prominent Areas.

Kim, H. I., & Han, K. Y. (2020). Urban flood prediction using deep neural network with data augmentation. *Water*, *12*(3), 899.

Kumar, A., Islam, T., Sekimoto, Y., Mattmann, C., & Wilson, B. (2020). Convcast: An embedded convolutional LSTM based architecture for precipitation nowcasting using satellite data. *Plos one*, *15*(3), e0230114.

Kumar, B., Chattopadhyay, R., Singh, M., Chaudhari, N., Kodari, K., & Barve, A. (2021). Deep learning–based downscaling of summer monsoon rainfall data over Indian region. *Theoretical and Applied Climatology*, *143*, 1145-1156.

Lakew, H. B., & Moges, S. A. (2021). Comparison of Spatial Interpolation Techniques of Rainfall for Hydrological Applications in a Complex Mountainous Region of the Upper Blue Nile Basin. *Nile and Grand Ethiopian Renaissance Dam: Past, Present and Future*, 461-474.

Li, Z., & Demir, I. (2022). A comprehensive web-based system for flood inundation map generation and comparative analysis based on height above nearest drainage. Science of The Total Environment, 828, 154420.

Li, Z., & Demir, I. (2023). U-net-based semantic classification for flood extent extraction using SAR imagery and GEE platform: A case study for 2019 central US flooding. Science of The Total Environment, 869, 161757.

Liu, Z., Shie, C. L., Li, A., & Meyer, D. (2020). NASA global satellite and model data products and services for tropical meteorology and climatology. *Remote Sensing*, *12*(17), 2821.

Lucas, M. P., Longman, R. J., Giambelluca, T. W., Frazier, A. G., Mclean, J., Cleveland, S. B., ... & Lee, J. (2022). Optimizing automated kriging to improve spatial interpolation of monthly rainfall over complex terrain. *Journal of Hydrometeorology*, *23*(4), 561-572.

Moishin, M., Deo, R. C., Prasad, R., Raj, N., & Abdulla, S. (2021). Designing deep-based learning flood forecast model with ConvLSTM hybrid algorithm. *IEEE Access*, *9*, 50982-50993.

Muckley, L., & Garforth, J. (2021). Multi-input convlstm for flood extent prediction. In *Pattern Recognition. ICPR International Workshops and Challenges: Virtual Event, January 10–15, 2021, Proceedings, Part VI* (pp. 75-85). Springer International Publishing.

Parker, J. A., Kenyon, R. V., & Troxel, D. E. (1983). Comparison of interpolating methods for image resampling. *IEEE Transactions on medical imaging*, *2*(1), 31-39.

Parsania, P. S., & Virparia, P. V. (2016). A comparative analysis of image interpolation algorithms. *International Journal of Advanced Research in Computer and Communication Engineering*, *5*(1), 29-34.

Peng, S., Ding, Y., Liu, W., & Li, Z. (2019). 1 km monthly temperature and precipitation dataset for China from 1901 to 2017. *Earth System Science Data*, *11*(4), 1931-1946.

Plouffe, C. C., Robertson, C., & Chandrapala, L. (2015). Comparing interpolation techniques for monthly rainfall mapping using multiple evaluation criteria and auxiliary data sources: A case study of Sri Lanka. Environmental Modelling & Software, 67, 57-71.

Sa, Y. (2014, October). Improved bilinear interpolation method for image fast processing. In *2014 7th International Conference on Intelligent Computation Technology and Automation* (pp. 308-311). IEEE.

Sermet, Y., & Demir, I. (2021). A semantic web framework for automated smart assistants: A case study for public health. Big Data and Cognitive Computing, 5(4), 57.

Sermet, Y., & Demir, I. (2022). GeospatialVR: A web-based virtual reality framework for collaborative environmental simulations. Computers & geosciences, 159, 105010.

Shah, M., Thakkar, A., & Shastri, H. (2023, January). A Comparative Study of Spatial Interpolation Methods for CMIP6 Monthly Historical and Future Hydro-climatic Datasets for Indian Region. In *2023 International Conference on Machine Intelligence for GeoAnalytics and Remote Sensing (MIGARS)* (Vol. 1, pp. 1-4). IEEE.

Shi, X., Chen, Z., Wang, H., Yeung, D. Y., Wong, W. K., & Woo, W. C. (2015). Convolutional LSTM network: A machine learning approach for precipitation nowcasting. *Advances in neural information processing systems*, *28*.

Skoulikaris, C., Venetsanou, P., Lazoglou, G., Anagnostopoulou, C., & Voudouris, K. (2022). Spatio-temporal interpolation and bias correction ordering analysis for hydrological simulations: an assessment on a Mountainous River Basin. *Water*, *14*(4), 660.

Sit, M., Seo, B. C., & Demir, I. (2021a). Iowarain: A statewide rain event dataset based on weather radars and quantitative precipitation estimation. arXiv preprint arXiv:2107.03432.

Sit, M., Demiray, B., & Demir, I. (2021b). Short-term hourly streamflow prediction with graph convolutional gru networks. arXiv preprint arXiv:2107.07039.

Sit, M., Seo, B. C., & Demir, I. (2021c). CNN-based Temporal Super Resolution of Radar Rainfall Products. arXiv preprint arXiv:2109.09289.

Sit, M. A., Seo, B., & Demir, I. (2023). TempNet–temporal super-resolution of radar rainfall products with residual CNNs. *Journal of hydroinformatics*, *25*(2), 552-566.

Timothy, D. (2016). Incorporating nesterov momentum into adam. *Natural Hazards*, *3*(2), 437-453.

Wang, S., Garcia, M., Ibrom, A., & Bauer-Gottwein, P. (2020). Temporal interpolation of land surface fluxes derived from remote sensing–results with an unmanned aerial system. *Hydrology and Earth System Sciences*, *24*(7), 3643-3661.

Yesilkoy, O. B. (2020). Prediction of commonly used drought indices using support vector regression powered by chaotic approach. *Italian Journal of Agrometeorology*, (2), 65-76.

Yeşilköy, S., & Şaylan, L. (2022). Spatial and temporal drought projections of northwestern Turkey. Theoretical and Applied Climatology, 149(1-2), 1-14.

Yildirim, E., & Demir, I. (2022). Agricultural flood vulnerability assessment and risk quantification in Iowa. Science of The Total Environment, 826, 154165.

Zhang, Z. (2018). *Image series prediction via convolutional recurrent neural networks with limited training data* (Doctoral dissertation, State University of New York at Binghamton).

URL 1: https://giovanni.gsfc.nasa.gov/giovanni/#service=TmAvMp&starttime=&endtime=

URL 2: https://code.mpimet.mpg.de/projects/cdo